Technische Universiteit Delft
Faculteit Elektrotechniek, Wiskunde en Informatica
Faculteit Technische Natuurwetenschappen
Delft Institute of Applied Mathematics

Pulse optimization for multi-qubit gates in transmon systems

Verslag ten behoeve van het
Delft Institute of Applied Mathematics
als onderdeel ter verkrijging

van de graad van

BACHELOR OF SCIENCE
in
TECHNISCHE WISKUNDE en
TECHNISCHE NATUURKUNDE door

Jorrit Hortensius

Delft, Nederland
Juni 2015

BSc verslag TECHNISCHE WISKUNDE en TECHNISHCE NATUURKUNDE

"Pulse optimization for multi-qubit gates in transmon systems"

Jorrit Hortensius

Technische Universiteit Delft

Begeleiders

Dr. A. Akhmerov
Dr. J. Dubbeldam

Overige commissieleden

Dr. L. DiCarlo

Dr. M. van Gijzen

Juni, 2015

Delft

Abstract

In transmon qubits, the leading source of errors for quantum gates is the existence of higher energy levels, besides the $|0\rangle$ and $|1\rangle$ states which form the computational subspace. Several methods have been developed to eliminate these errors systematically by clever use of the available experimental controls. In this bachelor thesis we focus on performing quantum gates on multiple qubits simultaneously, when transition frequencies of different qubits are close to each other. This approach should give a speed-up compared to the existing solution, which is designed to perform one quantum gate at the time, while eliminating all the effects on the other qubit. We develop a procedure to create new analytic pulse shapes which produce low-error gates for single qubits and we generalize this approach to multi-qubit systems to apply multiple quantum gates at the same time. For both single- and two-qubit gates these new pulses reduce errors by several orders of magnitude compared to simple driving pulses. In addition we combine these optimal analytical pulse shapes with multi-parameter pulses. The parameters of this additional pulse are optimized numerically, to produce even lower gate errors.

Contents

1 Introduction

The field of quantum computing studies computation systems in which quantum-mechanical phenomena such as superposition are used. These computation systems are often referred to as *quantum computers*. In classical computation systems, all data is processed and stored using bits. A bit is a binary digit which can have two values, which are often represented by 0 and 1. The building blocks of the quantum computers are qubits, the quantum computer analogs of classical bits. Whereas classical bits can only have one value at the time, qubits can be in a superposition of a $|0\rangle$ and $|1\rangle$: $|\psi\rangle = \alpha|0\rangle + \beta|1\rangle$. $\psi\rangle$ is referred to as the *state* of the qubit. α and β are complex numbers such that $|\alpha|^2 + |\beta|^2 = 1$. The $|0\rangle$ state of a qubit can be associated with the 0 for a classical bit, while the $|1\rangle$ state corresponds to a classical bit with value 1. Quantum computers promise to speed up computation by using the quantum-mechanical properties of these qubits.
Several research groups at the faculty of Applied Science of the Technical University of Delft work on different approaches to realize a working quantum computer. This is definitely not an easy task. As we said before, quantum qubits form the very base of quantum computers. Initializing and manipulating qubits as easily as classical bits is needed to build a quantum computer. In order to know how to manipulate qubits, we need to look into today's systems which are used as qubits. The standard example of a naturally occurring two-level (energy) system is a spin-$\frac{1}{2}$ particle, for example an electron. The spin-state can be controlled by applying an external magnetic field. Some research focuses on these true two-level systems such as trapped ions systems [1] and electrons in quantum dots [2]. Many present-day qubits in experimental research are in fact multi-level energy systems such as the transmon qubits, based on superconductive circuits with Josephson junctions [3]. These multi-level energy systems are often weakly anharmonic oscillators and are more easily controlled and isolated than the two-level systems. For instance, transmon qubits can be controlled with microwaves while still having long coherence times. However, the extra energy-levels also introduce new problems, because the system can leave the computational (qubit) subspace, which unavoidably leads to errors in the quantum computation. Logic operations, called quantum gates, on transmon qubits are induced by applying electromagnetic pulses to the circuits, which are in resonance with the energy difference between the different energy-levels of the qubit. For this reason it is essential that the system is an anharmonic oscillator. In a harmonic oscillator higher states would easily be excited, because of the equal spacing between all adjacent energy levels. In practice, to realize quantum algorithms, many qubits will have to be driven at the same time. This means that the resonance frequencies of these qubits have to be close to each other, because the frequency spectrum which is available for driving the qubits is limited. This leads to a second problem: when one qubit is driven, other qubits are automatically driven as well. The current solution (named Wah-Wah) is to perform a quantum gate on one qubit, while eliminating all effects on the second qubit. After that, the process is reversed and a quantum gate on the second qubit can be performed.
In this bachelor thesis we will focus on applying quantum gates on multiple qubits simultaneously, for qubits whose driving frequencies are close. This means that we want to combine the two steps of Wah-Wah and control multiple qubits at the same time, while dealing with the problems for multi-level energy systems which we described. Without loss of generality, we focus on performing an X gate on qubits, which are the quantum mechanical equivalent the classical NOT gates. The basic strategy is to adjust the electromagnetic pulses in such a way that the errors are decreased and the final quantum gates (final states of the qubit) are as close as possible to the desired ones.

The structure of the thesis is the following. In Chapter 2 we will give the background theory which is needed to understand how transmon qubits are manipulated and what the origin of the errors is. In Chapter 3 we explain an analytical approach based on the Dyson series, which we will use to improve multi-qubit gates. We combine this analytical technique with numerical optimization in Chapter 4. In addition we present the results of the combination of approaches in this chapter and compare them to existing solutions.

2 Formalism of transmon qubits and prior approaches

Qubits are the building blocks of the quantum computer, just as bits are for the classical computer. It is important to know how transitions between the $|0\rangle$ and $|1\rangle$ level can be induced for these qubits. Inducing such transitions, is called performing a quantum (logic) gate on the qubit. In this chapter we introduce the type of qubit on which this project is focused, we explain how quantum gates are performed and why (computational) errors occur.

2.1 Transmon qubits

In this thesis we focus on multi-level structures, such as the transmon qubit [3], a special type of a Josephson junction qubit. To understand the essence of a transmon qubit, we start with the simple quantum LC circuit. This is an electrical circuit which consists of an inductor (L) and a capacitor (C). This system can be quantized the same way as the harmonic oscillator, which has a parabolic potential energy. The result is that a quantum LC circuit has evenly spaced energy levels, which is illustrated in Fig. 1b. This situation is not optimal for the qubit, because all energy levels are seperated by the same frequency and therefore all energy levels can easily be excited at the same time. The solution to this problem is to replace the inductor L with a different component, namely a Josephson junction. This new circuit containing the Josephson junction is represented schematically in Fig. 1c. The role of the Josephson junction is to make the potential energy non-parabolic. As a result, the new system is an anharmonic oscillator with closer spaced levels for high energy (Fig. 1d)

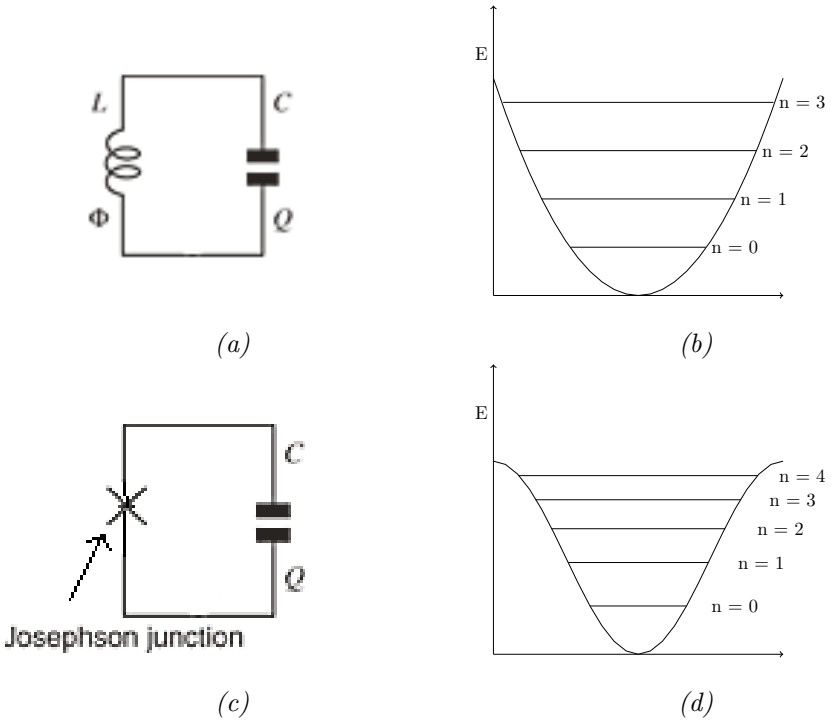

Figure 1: The quantum LC-circuit (a) and its energy spectrum with equally spaced energy levels (b). The circuit with the Josephson junction (c) has a non-parabolic potential and closed spaced levels for high energy (d).

2.2 Qubit model

A true qubit only has two energy levels, which correspond to the classical 0 and 1 state of a classical bit. In practice, physical systems have an infinite number of energy levels, like the transmon qubit. However, because the transmons are typically manipulated at temperatures (energies) much lower than the main transition frequency, we can use a simple model of an anharmonic oscillator having only three different energy levels, $|0\rangle$, $|1\rangle$ and $|2\rangle$. The first two levels, form the computational subspace, while the third level is the leakage level. This is the simplest model which can incorporate the effect of leakage on a qubit.
The ground state energy is set to zero, while the energy of the first and second excited state are $\hbar\omega_1$ and $\hbar\omega_2$. In this project we want to look at leakage to the second excited state and therefore we write $\omega_2 = 2\omega_1 + \Delta$, where Δ denotes the anharmonicity of the system. The Hamiltonian for this system is given by

$$\hat{H}_0 = \hbar(\omega_1\Pi_1 + \omega_2\Pi_2) \tag{2.1}$$

The model is illustrated in figure 2.

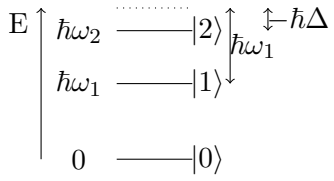

Figure 2: The different energy levels of the qubit and their corresponding energy(gaps)

For an isolated system at rest, these three energy levels are the so called eigenstates. This means that once a system is in one of these eigenstates, it will stay in that state. Under the influence of external electromagnetic fields this is no longer true, the system can shift between the different levels. The presence of the electric fields modifies the Hamiltonian which now becomes:

$$\hat{H} = \hat{H}_0(t) + \hbar\Omega(t)\left(\sigma_1^+ + \sigma_1^- + \lambda(\sigma_2^+ + \sigma_2^-)\right), \tag{2.2}$$

where: $\sigma_j^+ = |j\rangle\langle j-1|$, $\sigma_j^- = |j-1\rangle\langle j|$ and $\Pi_j = |j\rangle\langle j|$. When this Hamiltonian is written in matrix form, using the energy states $|j\rangle$ ($j \in \{0,1,2\}$) of the qubit as basis, it gives:

$$\hat{H}^{RF} = \hbar\begin{pmatrix} 0 & \Omega(t) & 0 \\ \Omega(t) & \omega_1 & \lambda\Omega(t) \\ 0 & \lambda\Omega(t) & \omega_2 \end{pmatrix}. \tag{2.3}$$

λ is an indicator of the relative strength of the $1 \leftrightarrow 2$ transition compared to the $0 \leftrightarrow 1$ transition. The value $\lambda = \sqrt{2}$ used throughout the thesis, unless specified otherwise. $\Omega(t)$ is the pulse which is applied to the system which will be of the following form, where w_d is the driving frequency:

$$\Omega(t) = \begin{cases} \Omega^x(t)\cos(\omega_d t) + \Omega^y(t)\sin(\omega_d t) & : 0 \le t \le T \\ 0 & : \text{elsewhere} \end{cases}$$

The Ω^x control is referred to as the in-phase-quadrature, while the Ω^y control is called the out-of-phase quadrature. T is the total gate time, the time during which a non-zero pulse

is applied.
To simplify the calculation it is convenient to go to the so-called interaction frame. This is done by applying the following time-dependent unitary transformation,

$$\hat{U}(t) = \Pi_0 + e^{i\omega_1 t}\Pi_1 + e^{i\omega_2 t}\Pi_2. \tag{2.4}$$

The Hamiltonian transforms as [see Appendix A]

$$\hat{H}^{RF} = \hat{U}\hat{H}\hat{U}^\dagger + i\hbar\dot{\hat{U}}\hat{U}^\dagger. \tag{2.5}$$

When this transformation is used to find the Hamiltonian in the rotating frame, we get the following result after applying the rotating wave approximation (RWA) [see appendix B] to neglect the fast oscillating terms:

$$\hat{H}^{RF} = \frac{\hbar}{2}\left[\Omega_C^\dagger(t)e^{-i\delta_1 t}\sigma_1^+ + \lambda\Omega_C^\dagger(t)e^{-i\delta_2 t}\sigma_2^+\right] + \text{h.c.}, \tag{2.6}$$

where h.c. stands for hermitian conjugate and

$$\Omega_C = \Omega^x + i\Omega^y$$
$$\delta_j = \omega_j - \omega_d.$$

When this Hamiltonian is written in matrix form, using the energy states $|j\rangle$ ($j \in \{0, 1, 2\}$) of the qubit as basis, it gives:

$$\hat{H}^{RF} = \frac{\hbar}{2}\begin{pmatrix} 0 & \Omega_C^\dagger(t)e^{-i(\omega_1-\omega_d)t} & 0 \\ \Omega_C(t)e^{i(\omega_1-\omega_d)t} & 0 & \lambda\Omega_C^\dagger(t)e^{-i(\omega_1+\Delta-\omega_d)t} \\ 0 & \lambda\Omega_C(t)e^{i(\omega_1+\Delta-\omega_d)t} & 0. \end{pmatrix} \tag{2.7}$$

When an electromagnetic driving pulse is applied, the qubit undergoes an evolution. The time evolution can be described by the time propagator $U(t, t_0)$, which satisfies the following differential equation:

$$\frac{d}{dt}U(t, t_0) = -\frac{i}{\hbar}H(t)U(t, t_0), \quad U(t = t_0) = 1. \tag{2.8}$$

The solution to this equation is [4]:

$$U(t, t_0) = \mathcal{T}\exp\left[\frac{-i}{\hbar}\int_{t_0}^{t} H^{RF}\mathrm{d}t'\right]. \tag{2.9}$$

In this equation, $\mathcal{T}$ is the time ordering operator. The origin of the need for this operator lies in the fact that for the matrix exponential, $e^{A+B} = e^A e^B$ is only valid if A and B commute.
A different expression for the solution is given by the Dyson series [5],

$$\begin{aligned} U(t, t_0) &= 1 - \frac{i}{\hbar}\int_{t_0}^{t}\mathrm{d}\,t_1 H(t_1) - \frac{1}{\hbar}\int_{t_0}^{t}\mathrm{d}\,t_2 H(t_2)\int_{t_0}^{t_2}\mathrm{d}\,t_1 H(t_1) \\ &\quad + \frac{i}{\hbar}\int_{t_0}^{t}\mathrm{d}\,t_3 H(t_3)\int_{t_0}^{t_3}\mathrm{d}\,t_2 H(t_2)\int_{t_0}^{t_2}\mathrm{d}\,t_1 H(t_1) + ... \\ &= U_0(t, t_0) + U_1(t, t_0) + U_2(t, t_0) + U_3(t, t_0) + ... \end{aligned} \tag{2.10}$$

To understand which driving pulses can be used as ideal starting point to perform a certain quantum gate, we can now simplify the Hamiltonian. We assume resonance between the driving frequency ω_d and the qubit frequency ω_1, which means that $\omega_1 = \omega_d$. In addition we set $\lambda = 0$. Physically, this means that the second excited state is left out and that only the two computational states of the qubit are considered.
Using the σ_1^+ and σ_1^-, which we defined before and the simplifications we rewrite equation (2.2) using the identities: $\sigma_{j,k}^x = |k\rangle\langle j| + |j\rangle\langle k|$ and $\sigma_{j,k}^y = i|k\rangle\langle j| - i|j\rangle\langle k|$
This leaves us with:

$$\hat{H}^{RF}(t) = \frac{\hbar}{2}\left(\Omega^x(t)\sigma_{0,1}^x + \Omega^y(t)\sigma_{0,1}^y\right). \tag{2.11}$$

In this project we mainly look at so called Pauli X-gates, which are the quantum equivalent of classical NOT-gates. When a not gate is performed on a classical bit, its value will change from a 0 to a 1 or vice versa. In the computational subspace of the qubit, this gate has the following matrix form:

$$X = \begin{pmatrix} 0 & 1 \\ 1 & 0 \end{pmatrix} \tag{2.12}$$

Therefore, this gate is exactly the same as the $\sigma_{0,1}^x$ operator. The overall phase of the qubit is not important and an additional phase shift is allowed on the leakage level. This gives for the quantum gate on the complete system, including the leakage level:

$$U_{ideal} = e^{i\phi_1}\begin{array}{c} \begin{matrix} |0\rangle & |1\rangle & |2\rangle \end{matrix} \\ \begin{pmatrix} 0 & 1 & 0 \\ 1 & 0 & 0 \\ 0 & 0 & e^{i\phi_2} \end{pmatrix} \end{array} \begin{matrix} |0\rangle \\ |1\rangle \\ |2\rangle \end{matrix}. \tag{2.13}$$

If we set $\Omega^y = 0$ and $\Omega^x = \Omega_\pi$, where $\Omega_\pi(t)$ can be any pulse which satisfies

$$\int_0^{t_g} \Omega_\pi(t')\,\mathrm{d}t' = \pi, \tag{2.14}$$

the Hamiltonians commute at all different times t_1 and t_2 [see appendix C]

$$[H^{RF}(t_1), H^{RF}(t_2)] = 0.$$

From this it follows that the time ordering operator $\mathcal{T}$ can be dropped in equation (2.9) in this specific case. This leaves us with

$$\begin{aligned} U_{\text{final}} &= \exp\left[\frac{-i}{\hbar}\int_0^T H^{RF}\mathrm{d}t'\right] \\ &= \exp\left[\frac{-i}{2}\pi\sigma_{0,1}^x\right] \\ &= iX \end{aligned} \tag{2.15}$$

The overall phase factor i, which comes with this final gate is not important.

2.3 Imperfect gates

In general $\lambda \neq 0$, which means that while we try to implement the NOT gate, the unwanted result can be that the system gets excited to a superposition containing the

third energy state. This is a serious problem, since for a quantum computer, all qubit operations (quantum gates) have to be performed with high precision, just as in normal computers. It is very hard to perform near-perfect quantum gates in short times. We can immediately see that these errors are the result of the nonzero terms associated with the $1 \leftrightarrow 2$ transition in the Hamiltonian in equation (2.7) (which in turn result from the presence of a third energy level). Because of the finite gate time T, the Fourier spectrum of the pulse necessarily has a finite frequency bandwidth. The Fourier spectrum is centered around the driving frequency ω_d, but it is nonzero at frequencies close to ω_d, so that the component at the frequency of the $1 \leftrightarrow 2$ transition ($\omega_2 - \omega_1 = \omega_1 + \Delta$) is nonzero. This is the reason that the driving pulse drives the $1 \leftrightarrow 2$ transition in the system as well.
The problems with leakage, due to unwanted driving of the $1 \leftrightarrow 2$ transition, apply to systems of multiple qubits as well. For simplicity we start by looking at two qubits. The situation is illustrated in Fig. 3 below. In total there are now four possible transitions. The goal is to implement a qubit gate on both qubits (with low errors) at the same time.

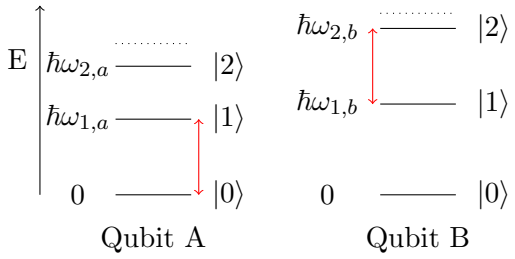

Figure 3: A schematic overview of the qubit model for a system of two qubits

In addition certain transitions such as the $0 \leftrightarrow 1$ transition of qubit A and the $1 \leftrightarrow 2$ transition of qubit B can be close to each other. When we call the spacing between these transitions δ_{AB}, $\delta_{\mathrm{AB}} = (\omega_{2,b} - \omega_{1,b}) - (\omega_{1,a} - 0)$, we can easily have $|\delta_{\mathrm{AB}}| < |\Delta|$. So driving qubit A can lead to large leakage in qubit B, because in experiments multiple qubits are often coupled to a common feedline used for transmitting the driving pulse. This cross-driving causes the main errors in applying quantum gates simultaneously to multiple qubits.

2.4 Gate fidelity

To quantify this error which is present in the final qubit gate for pulses which drive a single qubit, we use the gate fidelity. This is a measure for how close the final quantum gate is to the ideal gate. The way to calculate this fidelity is to see how close the final state is to the desired state, by taking the overlap (squared inner product) of these two states, for each possible initial state in the two-dimensional Hilbert space. This seems to be a very difficult task, but using an argument which is explained in [6], it is sufficient to calculate the fidelity over the six main directions of the Bloch sphere. The formula for the gate-fidelity becomes after some rewriting:

$$F_g = \frac{1}{6} \sum_{j=\pm x,\pm y,\pm z} \left| \left\langle \psi_j | U_{\mathrm{ideal}}^{\dagger} U_{\mathrm{final}} | \psi_j \right\rangle \right|^2, \tag{2.16}$$

where U_{ideal} is the unitary (gate) which we want to create, $|\psi_j\rangle, j \in \{\pm x, \pm y, \pm z\}$ are the six axial pure states of the Bloch sphere and U_{final} is the actual final quantum gate which

is performed. With this definition for the gate fidelity, the performed gate is perfect if the fidelity is equal to 1. Hence, the error can be quantified as $1 - F_g$.

2.5 Existing solutions

2.5.1 Single qubits

To avoid large leakage into the third energy level, in practice pulse shapes with small frequency bandwidths are used. A very commonly used pulse shape is a Gaussian shape [7], which has a small frequency bandwidth:

$$\Omega^x(t) = Ae^{-\frac{(t-\frac{t_g}{2})^2}{2\sigma^2}} - B. \tag{2.17}$$

In this equation, σ is the standard deviation corresponding to the Gaussian. A and B are chosen in such a way that the pulse Ω^x starts and ends at zero and meets the requirement 2.14. For long gate times the effect of the third level is much smaller, because the weight of the pulse at the leakage frequency becomes smaller. The longer the gate time T is, the smaller the bandwidth of the pulse. This effect is illustrated in Fig 4. For large gate times, the error becomes small, even for the simple Gaussian pulse.
Even though using Gaussian pulse shapes diminishes the leakage to the third energy level, simulations show that the errors caused by this extra energy level are still significant ($> 1\%$) for short gate times of 10 ns . To solve this problem, in Ref. [8] the so-called DRAG technique (Derivative Removal via Adiabatic Gate) was introduced, which prescribes a certain group of pulses for single qubit gates with lower gate errors than simple Gaussian pulses. The main structure of these optimized pulses is as follows:

$$\begin{aligned} \Omega^x &= Ae^{-\frac{(t-\frac{t_g}{2})^2}{2\sigma^2}} - B \\ \Omega^y &= \beta\dot{\Omega^x} \end{aligned} \tag{2.18}$$

On the in-phase quadrature a standard pulse envelope is used, while on the out-of-phase quadrature the derivative of this envelope is applied.

In the derivation of the DRAG technique, the effective Hamiltonian for a single qubit as a result of a simple Gaussian pulse is approximated. This technique is based on an adiabatic expansion in the small parameter $\frac{\Omega^x}{\Delta}$. In the adiabatic limit of very long gate times (low pulse amplitudes), or large anharmonicity Δ, a simple pulse as described in (2.17) gives a very accurate $\sigma^x_{0,1}$ gate, even in the presence of a third energy level. This is illustrated in Fig. 4. The gate error for the resulting qubit gate decreases with increasing gate times. This means that DRAG is some sort of first order correction which tries to correct for the presence of the leakage level. For this first order correction, $\beta = -\frac{1}{\Delta}$ is chosen. Note that different versions of DRAG exist [9], and that this approach has been tested experimentally [10].

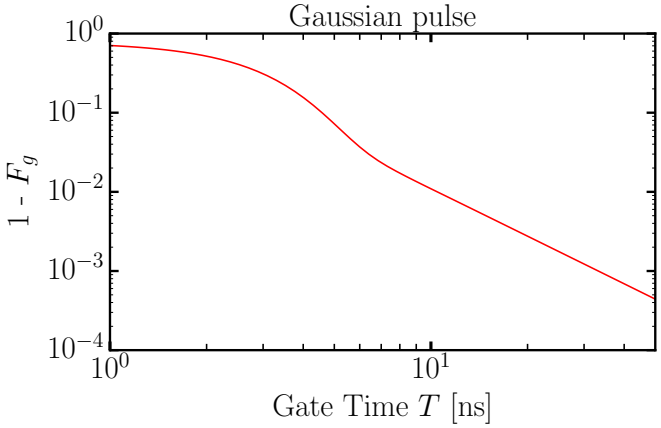

Figure 4: The gate error for a simple Gaussian pulse ($\sigma = \frac{T}{6}$). The qubit parameters which are used are $\lambda = \sqrt{2}$ and $\Delta = -400$ MHz $\cdot 2\pi$. These are realistic values for transmon qubits [11]

.

2.5.2 Multiple qubits

As a solution to the problem of cross-driving, so-called Wah-Wah control (Weak An-Harmonicity With Average Hamiltonian) has been developed [11]. Wah-Wah control uses a pulse with four parameters. It uses a Gaussian with added sideband modulation on the in-phase quadrature, together with a DRAG-like pulse (derivative) on the out-of-phase quadrature. The method is again derived from making an adiabatic expansion in the small parameter $\frac{\Omega^x}{\Delta}$. The goal is to apply a single qubit gate on one qubit, without affecting the second qubit. With this technique, high fidelities of 99.9% can be reached with gate time as short as 17 ns, while $\frac{\delta}{2\pi}$ is as small as 45 MHz. In comparison, simulations show that if a DRAG-like pulse of the same duration is used to cancel the leakage in qubit 2, it would give a gate fidelity of about 90 %. This technique has also been tested experimentally and led to average gate errors smaller than 1 % for gate times between 16 and 24 ns, while DRAG-like pulses caused significant leakage [12].

2.6 The next step: Multi-qubit gates

Even though Wah-Wah works quite well, it has the limitation that it can only be used to implement single-qubit gates. Indeed, its goal is to perform a quantum gate on one qubit, without affecting the second one. It would however be a great advantage to be able to perform quantum gates with low errors on multiple qubits simultaneously. This is difficult, since it means that internal leakage has to be prevented for each qubit, as well as leakage as result of driving the other qubits. The pulses driving the other qubits are 'off-resonant' pulses. In the next chapter, we develop a method based on the Dyson series to accomplish this task.

3 A different adiabatic expansion

3.1 Introduction

For performing multi-qubit logic gates, qubits at different frequencies have to be driven. This means that *polychromatic pulses* are needed, which are pulses at multiple driving frequencies. In the previous chapter we have seen that DRAG uses an adiabatic expansion to derive pulse envelopes which decrease the gate error. This approach motivates us to introduce a similar adiabatic expansion for arbitrary pulses at arbitrary driving frequencies. In this chapter we derive the effective Hamiltonian for a qubit, subject to arbitrary on-resonant or off-resonant pulses, by using the Dyson series. We then investigate numerically whether the expansion works as expected and use it to derive pulses for both single and multiple qubit gates. In the case of multiple qubits, we use as the target gate an X-gate ($\sigma^x_{0,1}$) to each qubit individually.

3.2 Effective Hamiltonian

The qubit model and driving by applying electromagnetic fields are described in section 2.2. This time we use a driving frequency ω_d which can be different from the qubit frequency ω_1. We define $\delta = \omega_1 - \omega_d$. Since the goal is to find low order non-adiabaticity corrections on simple existing pulses, we expand the time propagator $U(t, t_0)$ up to terms of order Ω^2, using the Dyson series (equation 2.10). Ω is in this case a parameter which scales with the average amplitude of the pulse envelope. We can do this because for pulses $\Omega_\pi(t)$ applied to perform a $\sigma^x_{0,1}$ gate, we know that it must satisfy requirement (2.14). Therefore we easily see that $\Omega \sim \frac{1}{T}$, where T is the total gatetime. Ω is therefore an adiabatic parameter. In the limit of very long gate times, the errors of $\mathcal{O}(\Omega^3)$ in the expansion go to zero.
Because the Hamiltonian in equation (2.7) is linear in Ω, it is enough to expand the Dyson series up to and including the term $U_2(t, t_0)$, while approximating the integrals with oscillating terms (exponents) in the following way using the Taylor expansion for $\Omega(t)$:

$$\int_{t_0}^{t} \Omega(t') e^{i\delta t'} \, \mathrm{d}t' \approx \int_{t_0}^{t} \Big(\Omega(t_0) + \dot{\Omega}(t_0)(t_1 - t_0) \Big) e^{i\delta t_1} \, \mathrm{d}t_1.$$

If $\Omega \sim \frac{1}{T}$, this means that $\frac{d}{dt}\Omega \sim \frac{1}{T^2} \sim \Omega^2$. This means that we can truncate the Taylor expansion of $\Omega(t)$ around t_0 in the integral after two terms. Further expansion of $\Omega(t)$ is not needed, since it will lead to terms of order $\mathcal{O}(\Omega^3)$.
In addition we approximate the time propagator $U(t_0 + t_p, t_0)$ for a certain time period t_p, which completely describes the time evolution of the qubit between $t = t_0$ and $t = t_0 + t_p$. At that point the expansion gives an expression for $U(t_0 + t_p, t_0)$ which is correct up to $\mathcal{O}(\Omega^2)$. To get the effective Hamiltonian H_{eff} from this expression we use the equation:

$$U(t_0 + t_p, t_0) \equiv e^{-\frac{i}{\hbar} H_{\text{eff}} \cdot t_p}, \tag{3.1}$$

which basically is the definition of an effective Hamiltonian H_{eff}. This means that

$$H_{\text{eff}}(t_0) = \frac{i\hbar}{t_p} \log(U(t_0 + t_p, t_0)). \tag{3.2}$$

Expression (3.2) can be approximated up to $\mathcal{O}(\Omega^2)$ as well using the Taylor expansion of the logarithm. This leads to

$$H_{\text{eff}}(t_0) \approx \frac{i\hbar}{t_p}\left(U_1 + U_2 + \frac{1}{2}(U_1 + U_2)^2\right), \tag{3.3}$$

where U_1, U_2, correspond to the first terms of the Dyson series. The complete derivation and approximation is explained in D and will be validated later numerically.
In the remaining of the chapter we will derive the effective Hamiltonian for different relevant cases. We start with the simple case of a resonant driving pulse. Then, we use the effective Hamiltonians to find pulses which perform quantum gates with lower errors for single and multiple qubits.

3.3 Resonant driving pulse

We start with the simple case in which $\delta = 0$, which means that the driving pulse is on resonance with the $0 \leftrightarrow 1$ transition of the qubit. There are a two important points:

- Ideally, the on resonant driving pulse only drives the $0 \leftrightarrow 1$ transition of the qubit. This means that for the ideal Hamiltonian (which corresponds to a perfect final gate) in the rotating frame, the only non-zero terms should be the ones corresponding to this transition.
- As a result, all other non-zero terms in the effective Hamiltonian are unwanted. For example a non-zero term on the [1,2]-entry of the effective Hamiltonian, means that the driving pulse effectively drives the $1 \leftrightarrow 2$ transition as well. Consequently there is a probability that the qubit leaves the computational subspace.

In this case, the Dyson series leads to the following expression for the (time-dependent) effective Hamiltonian, where we have substituted t for t_0

$$H_{\text{eff,on}}(t) = \hbar \begin{pmatrix} 0 & \frac{1}{2}\Omega^*(t) + \frac{t_p}{4}\dot{\Omega}_1^*(t) & -\frac{1}{4\Delta}\lambda_1\Omega^*(t)\Omega^*(t)e^{-i\Delta t} \\ \frac{1}{2}\Omega_1(t) + \frac{t_p}{4}\dot{\Omega}_1(t) & -\frac{1}{4\Delta}\lambda_1^2|\Omega_1(t)|^2 & \frac{i}{2\Delta}\lambda_1\dot{\Omega}_1^*(t)e^{-i\Delta t} \\ -\frac{1}{4\Delta}\lambda_1\Omega_1(t)\Omega_1(t)e^{i\Delta t} & -\frac{i}{2\Delta}\lambda_1\dot{\Omega}_1(t)e^{i\Delta t} & \frac{1}{4\Delta}\lambda_1^2|\Omega_1(t)|^2 \end{pmatrix}. \tag{3.4}$$

It is important to check if this expression makes sense and that this expansion in pulse amplitude Ω works. Therefore we do the following simulation, using a pulse with a Gaussian on the in-phase-quadrature. Ideally, this should lead to a $\sigma_{0,1}^x$ gate on the qubit.

To check whether our expansion works correctly, we compute the gate error for an artificial Hamiltonian, obtained by subtracting the unwanted terms appearing in the effective Hamiltonian in Eq. (3.4)), from the original qubit Hamiltonian in Eq. (2.7). Basically all terms in the expansion above are unwanted, except for the terms corresponding to the $0 \leftrightarrow 1$ transition. This new Hamiltonian is the result of subtracting terms from the originial Hamiltonian, during the simulations. This is not a physical Hamiltonian as a result of an electromagnetic pulse, hence we call it artificial Hamiltonian.
If the expansion works the way we expect, the 'artificial' Hamiltonian should cancel all unwanted effects of the Gaussian pulse up to second order. The unwanted effects therefore

become of $\mathcal{O}(\Omega^3) = \mathcal{O}(\frac{1}{T^3})$, with T again being the gate time. All unexpected effects of lower order should be canceled. The final gate is received after integrating the artificial Hamiltonian over time. The gate error scales with the squared error of the entries of the final unitary, which can be seen in equation (2.16). Combining all this gives that for the gate error:

$$1 - F_g = \mathcal{O}\left(\left(\frac{T}{T^3}\right)^2\right) = \mathcal{O}(\frac{1}{T^4})$$

In Fig (5) we see the gate errors of the final gates, as a result of the different Hamiltonians. The slope of the graph indicates with which power of T the error decreases. From this graph it follows that $1 - F_g \sim \frac{1}{T^4}$ for the gate as a result of the artificial Hamiltonian, which indicates that the expansion works as expected. With this, we mean that we can conclude that the effective Hamiltonian in equation (3.4) is correct up to $\mathcal{O}(\Omega^3)$. The gate error decreases faster than the gate error for the 'normal' Gaussian pulse. This indicates that lower gate errors could be obtained by designing a new pulse which eliminates the unwanted terms in the effective Hamiltonian.

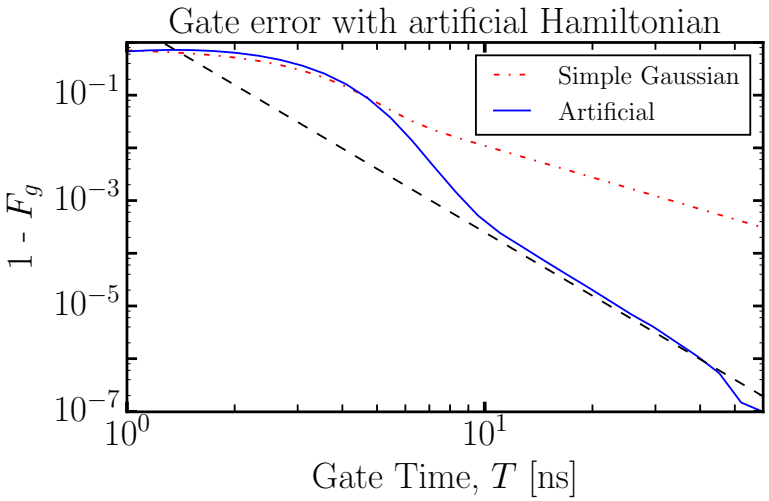

Figure 5: The gate error for a simple Gaussian pulse ($\sigma = \frac{T}{6}$), the red dash-dot line, compared to the error when all unwanted terms are substracted from the Hamiltonian (the blue solid line). The (black) dashed line is of the form $c\frac{1}{T^4}$, to show the rate with which the error of artificial pulse falls off.

We can also investigate which unwanted terms in the effective Hamiltonian cause the most error. The leakage errors due to the pulse (the non-zero entries for the $0 \leftrightarrow 2$ and $1 \leftrightarrow 2$ transitions in Eq. 3.4) are of a higher order (in the pulse amplitude) with respect to the phase error between the states $|0\rangle$ and $|1\rangle$, which is caused by the diagonal matrix elements. Ideally the difference between the H_{00} ([0,0]-entry) and H_{11} term should be zero.

A new artificial Hamiltonian is made, by only subtracting the error on the diagonal terms from the original Hamiltonian. The gate error of the final gate, which is a result of the evolution under this second artificial Hamiltonian is calculated. This is demonstrated in Fig. 6 below. The gate error falls off with the same rate as the situation for the 'full artificial Hamiltonian'. This indicates that the phase error is the most important among all unwanted terms in the effective Hamiltonian for reasonably large gate times

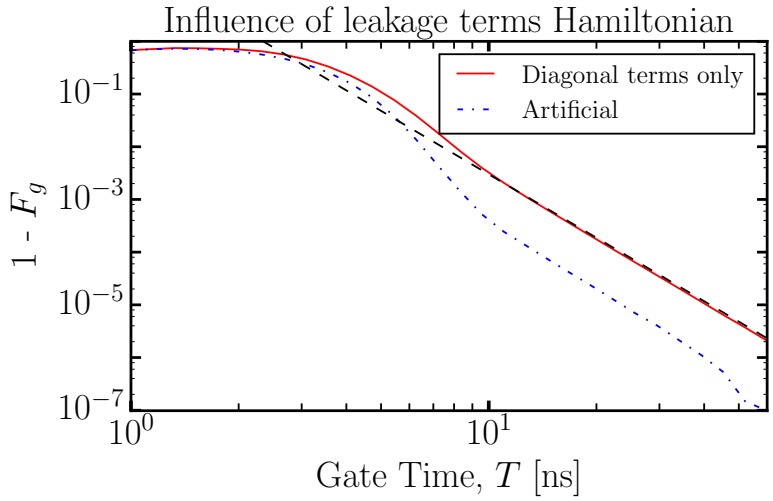

Figure 6: The gate error for the artificial pulse (blue solid line) is compared to the final error for the situation where only the unwanted diagonal terms (the phase error) appearing in the effective Hamiltonian (eq 3.4) are removed (red dot-dashed line). The black dashed line is graph of a function of the form $c\frac{1}{T^4}$, to show the rate with which the error of this phase-compensating pulse falls off.

From this point on, the main strategy is to correct the pulses by removing the unwanted terms, especially the ones which cause the phase error. This is the same approach as the DRAG-pulse [8].

3.4 Off resonant driving pulse

For an off resonant pulse, the same expansion can be made as in the previous section. In this case, $\delta \neq 0$. There is one important point:

- Ideally, the off resonant driving pulse does not influence the qubit, so it should not act on the qubit at all. The only pulse which should drive the qubit is an on-resonant driving pulse. This means that for the ideal effective Hamiltonian for an off-resonant pulse in the rotating frame, all terms should be equal to zero.

The calculation of the effective Hamiltonian is a little longer and gives the following result:

$$H_{\text{eff, off}}(t) = \hbar \begin{pmatrix} -\frac{1}{4}\frac{|\Omega_2|^2}{\delta} & \dot{\Omega}_2^*(t)e^{-i\delta t}\frac{i}{2\delta} & 0 \\ -\dot{\Omega}_2(t)e^{i\delta t}\frac{i}{2\delta} & \frac{1}{4}\frac{|\Omega_2|^2}{\delta} - \frac{\lambda_1^2|\dot{\Omega}_2|^2}{4(\delta+\Delta)} & \frac{1}{2}\lambda_1\dot{\Omega}_2^*(t)\frac{e^{-i(\Delta+\delta)t}}{-i(\delta+\Delta)} \\ 0 & \frac{1}{2}\lambda_1\dot{\Omega}_2^*(t)\frac{e^{i(\Delta+\delta)t}}{i(\delta+\Delta)} & \frac{\lambda_1^2|\Omega_2|^2}{4(\delta+\Delta)} \end{pmatrix} \tag{3.5}$$

Similarly to the on resonant pulse, we can numerically validate this expression. For an off-resonant pulse, all non-zero terms in the effective Hamiltonian are unwanted. The artificial Hamiltonian is therefore created by subtracting all terms in the effective Hamiltonian, from the normal Hamiltonian. $H_{\text{artificial}} = H_{\text{pulse}} - H_{\text{eff,off}}$, where H_{pulse} is given by Eq. (2.7)

We suspect that the induced phase difference between the $|0\rangle$ and $|1\rangle$ level has again the largest influence on the gate error. A new artificial Hamiltonian is made, by only subtracting the error on the diagonal terms from the original Hamiltonian (equation (2.7)). The gate error of the final gate, which is a result of the evolution under this second artificial Hamiltonian is calculated. This is demonstrated for two different values of δ in Fig. 7

below. For both values of δ, the error of the final gate calculated with the artificial Hamiltonian scales with $\frac{1}{T^6}$ for large gate times. This is a higher order than expected, since we calculated that the error should fall of with $\frac{1}{T^4}$. This might mean that the contribution of the third-order term of the Dyson series is negligible. When only the diagonal terms are removed, the gate error falls off with the same rate. Just like the situation for the on-resonant pulse, leakage seems to be less influential on the gate error than the phase difference within the computational subspace

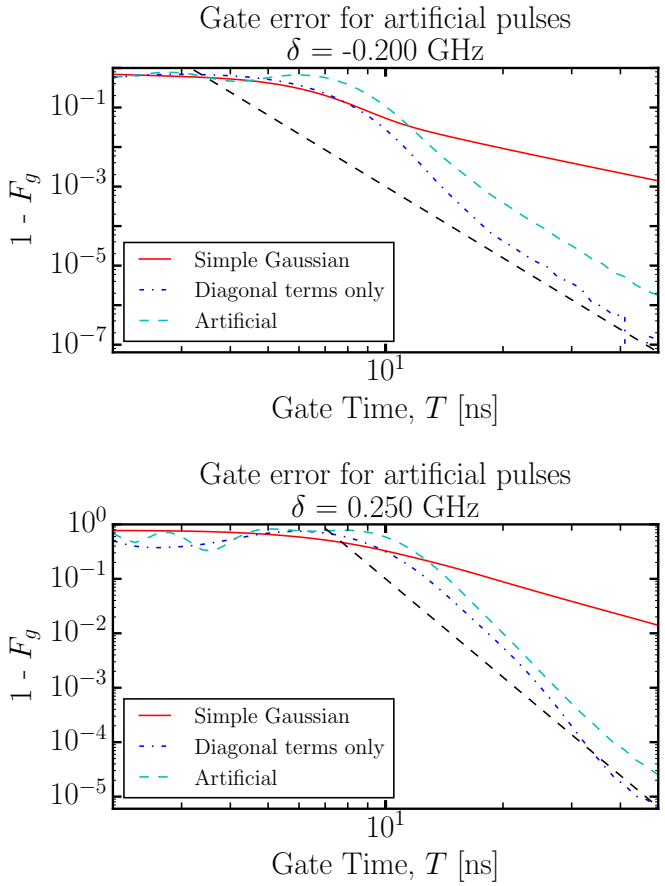

Figure 7: For two different values of δ, the influence of different error terms appearing in the effective Hamiltonian is investigated. The red (solid) line is the gate error as a result of a simple Gaussian pulse. The light blue dashed line shows the error for the artificial Hamiltonian. The blue dash-dot line is the result when only the diagonal terms are removed. This graph shows that only removing the diagonal terms leaves us with an error which scales with the error for the total artificial Hamiltonian

.

3.5 Phase ramping

We start with the simplest case: an simple Gaussian pulse Ω_1 which is in resonance with the qubit on the in-phase-quadrature, and no envelope on the out-of-phase-quadrature. $\Omega_1 = \Omega_1^x + i\Omega_1^y = \Omega_G + 0i$, where Ω_G denotes a Gaussian pulse. From the effective Hamiltonian (3.4) we see the total effect of this pulse. We now have to improve the pulse by removing unwanted effects. As demonstrated in Fig. 6, it is important to cancel the

phase error (H_{11} term) in the effective Hamiltonian. The pulse induces an undesired phase difference between the ground state and the first excited state of the qubit. As demonstrated in Ref. [8], this undesired phase difference can be compensated by applying a phase to the driving pulse, according to the equation:

$$\Omega_{\text{total}} = \Omega_t e^{i(\phi(t)-\phi(T)/2)}, \tag{3.6}$$

where

$$\phi(t) = \int_0^t \left(H_{11}(t') - H_{00}(t')\right)\, \mathrm{d}t' \tag{3.7}$$

and T is the gate time. This process is called phase ramping.

It is useful to compare the gate error of this resulting phase-compensating pulse with gate errors for the DRAG pulse and simple Gaussian pulses and see if neglecting the leakage is allowed. It turns out that not compensating for the leakage is a good choice. For the standard (theoretical) value of $\lambda = \sqrt{2}$, the gate error of the phase-compensating pulse are of the same order of magnitude as the errors for the DRAG pulse. This is in accordance with [9], since the optimal pulse in 3.6 is equivalent to an error-eliminating pulse which they call Z-only correction.

More importantly, when trying to correct for these leakage effects, for smaller values for λ, the gate error becomes larger than the error for the Gaussian pulse. This is illustrated in Fig. 8 below. The first order DRAG-pulse [8], which corrects for the phase difference between the $|0\rangle$ and $|1\rangle$ state and corrects for the leakage, does not work well for small values of λ.

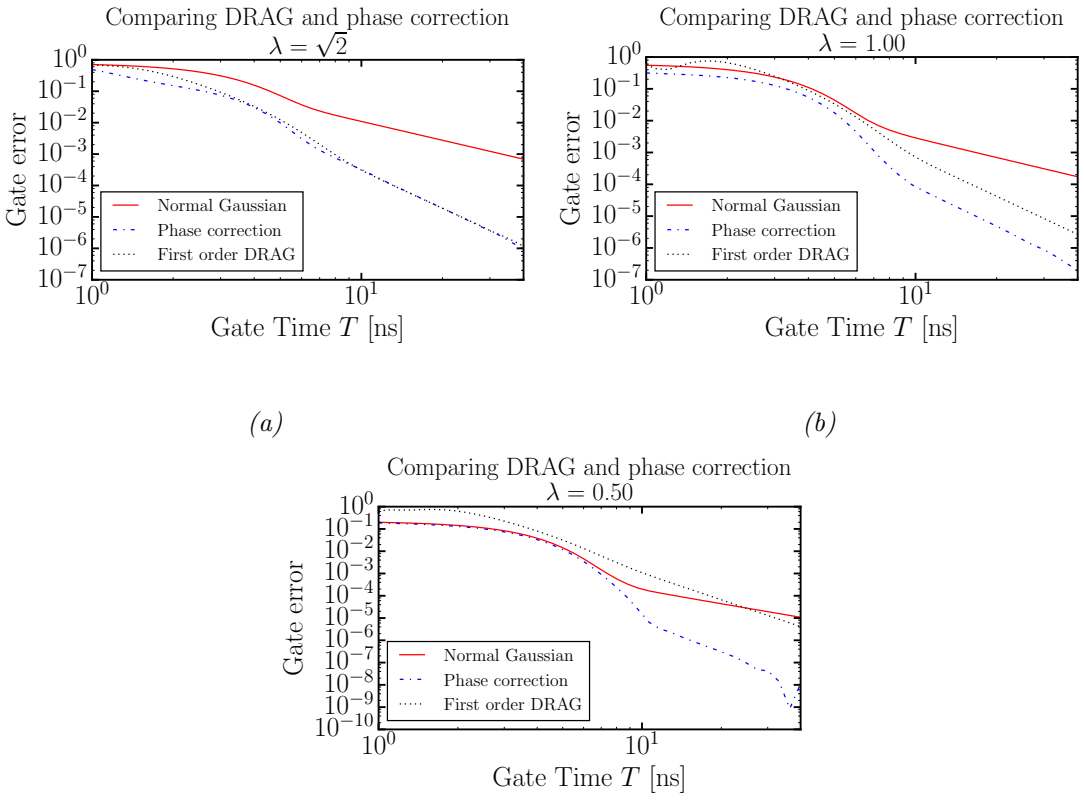

Figure 8: The gate error vs pulse duration for a simple Gaussian pulse ($\sigma = \frac{T}{6}$), the phase correction pulse and first order DRAG pulse, for $\lambda = \sqrt{2}(a)$, 1 $(b)$and $0.5(c)$. For $\lambda = 0.5$, the DRAG pulse does not show any improvement compared to the simple Gaussian pulse, while only applying phase correction does give lower gate errors.

We can draw an important conclusion. For single qubit gates, the gate error is dictated by the induced phase difference between the two computational states. The leakage to the third energy level does not contribute much to the error. The expansion of the effective Hamiltonian leads to a new pulse, which has gate errors as low as first order DRAG for gate times larger than 3 ns.

We can apply the same method to eliminate the (undesired) effects on the qubit as a result of off-resonant pulses. This is important in the multi-qubit systems described in section 2.3, where multiple qubits are driven at the same time. This is the first step in finding improved pulses which might produce low-error multi-qubit gates, using polychromatic pulses. We look at the following situation: On a given driving frequency ω_d, which is detuned from the qubit frequency by $\delta = \omega_d - \omega_{\text{qubit}}$, a simple Gaussian pulse is applied. The goal is to apply a low-error X-gate on the qubit, using a pulse on the qubit frequency w_{qubit} while dealing with this off-resonant pulse as well.
The gate error as a consequence of an off-resonant pulse is mainly the result of an induced phase difference between the $|0\rangle$ and the $|1\rangle$ state. This is what we showed in section 3.4. Therefore, to eliminate this phase effect, we apply the same solution as we used for on-resonant pulses. We start with a pulse Ω_{phase} which works well for applying an X-gate on a single qubit, equation (3.6). To compensate for the off resonant phase effect, we multiply the final pulse with a factor, which depends on the H_{00} and H_{11} terms (of the

effective Hamiltonian for an off-resonant pulse, equation (3.5)) :

$$\Omega_t = \Omega_{\text{phase}} e^{i(\phi(t)-\phi(T)/2)} \tag{3.8}$$

Where $\phi(t)$ is again given by Eq. 3.7, now using the terms from the Hamiltonian for the off-resonant pulse (Eq. (3.5)). In Fig. 9, the gate error for this improved pulse Ω_t is plotted versus the gate time T for two different detuning values δ. It is clear that for large gate times T the error for the new pulse is lower than for the simple Gaussian pulse. The gate error seems to fall off with $\mathcal{O}(\frac{1}{T^6})$ for large gate times, which confirms the presumption that only correcting for the induced phase difference removes the lowest order non-adiabaticity errors.

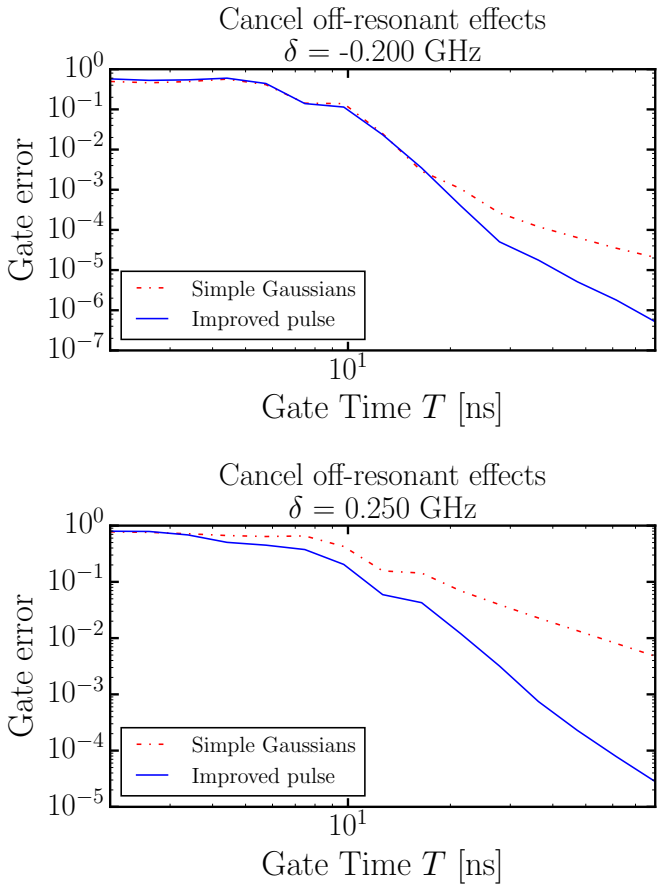

Figure 9: On the off-resonant driving frequency a simple Gaussian pulse is applied. On the qubit frequency (on-resonant pulse), the new improved pulse is applied. The error as a result of this combination of pulses is plotted against gatetime for detuning values δ = -0.2 GHz (a) and δ = 0.25 GHz (b) (blue, solid line). To compare, the error is plotted for the gate when a simple Gaussian pulse is used on the qubit frequency (red dash-dot line).

3.6 Multi-qubit X-gates

With all the ingredients available, it is possible to look at driving two qubits simultaneously. To begin with, we introduce a new setup of the qubits in frequency space. This is to avoid the very small separations δ_{AB} described in section 2.3. It seems more logical to have as many equal frequency seperations within the system as possible.

For two qubits A and B, each with an anharmonicity of $\Delta_{\mathrm{A}} = \Delta_{\mathrm{B}} = 2\pi \cdot -0.4$ GHz, this leads to the possible setups clarified in Fig. 10. It seems more logical to use the setup in 10a, but from numerical simulations it follows that our expansion breaks down as $\delta \to -\frac{\Delta}{2}$. The separation with $|\delta| = 0.2$ GHz $\cdot 2\pi = \frac{|\Delta|}{2}$, leads therefore to bad results. It is for this reason that from this point on we use the setup in figure 10b.

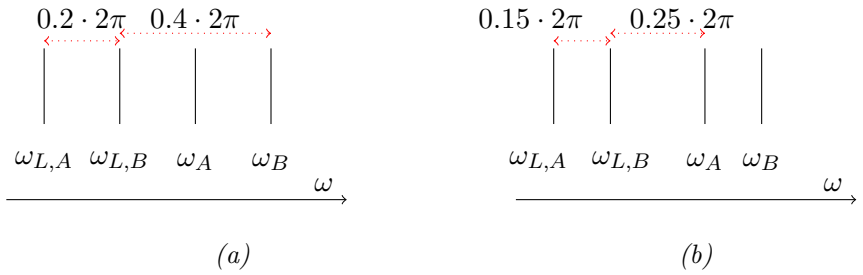

(a) *(b)*

Figure 10: A schematic overview of the new setups in frequency space. $\omega_{L,A}$ denotes the frequency of the $1 \leftrightarrow 2$ (leakage) transition of qubit A, while ω_A is the frequency of the $0 \leftrightarrow 1$ transition.

The idea is to apply on both qubits the off-resonant phase ramp pulse which we introduced in the previous section. This pulse tries to cancel the total error, which results from 'internal unwanted effects' and 'off resonant influences'. In Fig. 11 the gate error is plotted vs the gate time T. For both qubit A and B, the new pulses lead to lower gate errors at all gate times. At a gatetime of just 35 ns, the gate error is below 10^{-3} for both qubits.

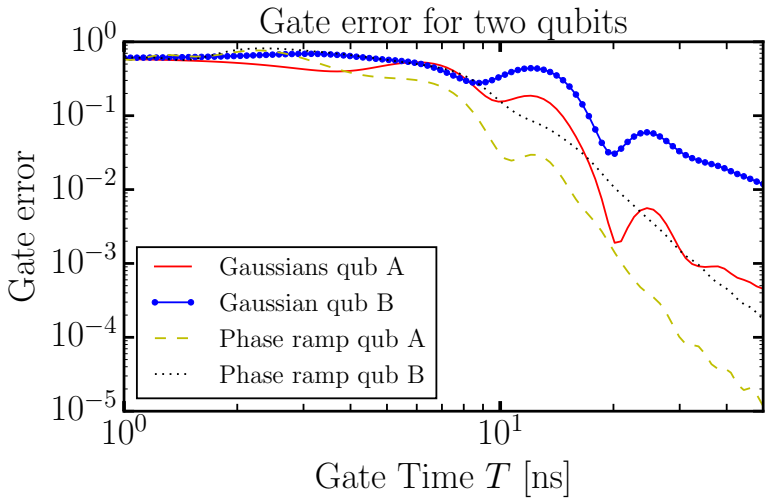

Figure 11: The gate error for the two qubits in two different situations. When two simple Gaussian pulses are applied on both qubits, it leads to the error for qubit A (red solid line) and qubit B (blue large dotted line). When the improved pulses are applied to the system, they lead to the new (lower) error for qubit A (yellow dashed line) and qubit B (black small dotted line)

The same idea has been applied to more than two qubits. For three qubits, the setup in frequency space is illustrated in Fig. 12.

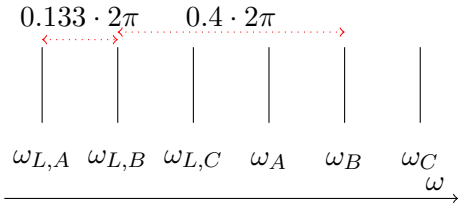

Figure 12: A schematic overview of the new setups in frequency space, for three qubits A, B and C. ω_i and $\omega_{L,i}$, i = 1,2,3 denote the main transition and leakage frequency.

The resulting gate errors for applying the improved phase ramping pulses are plotted in Fig. 13. The gate error is the highest for qubit C, since for this qubit there are driving pulses close to the leakage transition. The method of phase ramping does not seem to reduce the error much for qubit C. This indicates that for the situation of qubit C, the phase error is no longer the main source of error.

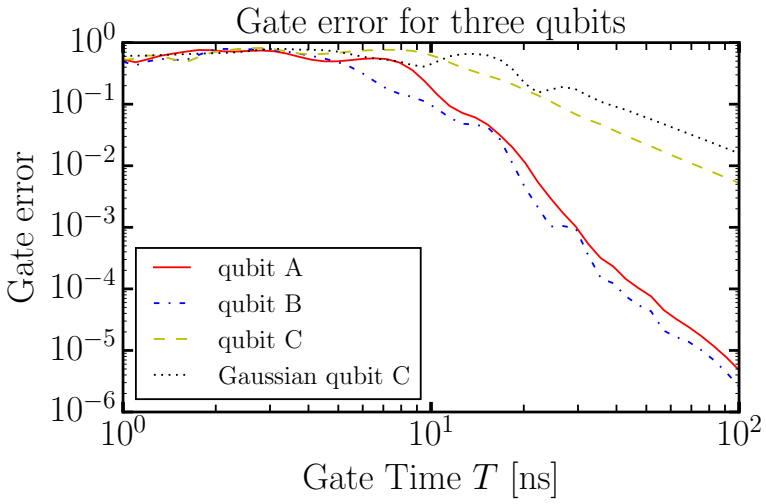

Figure 13: The gate error for three qubits. On each qubit frequency, an improved pulse is applied, which leads to the error for qubit A (red solid line), qubit B (blue large dotted line), qubit C (yellow dashed line). To compare, the error for qubit C is plotted, when on each frequency a simple Gaussian pulse is applied.

3.7 Discussion of the results

Whereas the expansion of the effective Hamiltonian leads to a pulse with very low error for a single qubit gate, the situation is harder for multiple qubits. Numerically, we see that the errors sensitively depend on the values of delta. In particular we have observed that the expansion does not work when $\delta \to \frac{-\Delta}{2}$. This might be due to errors introduced in the period-averaging performed during the calculation of the effective Hamiltonian. This is the reason why we have looked at the slightly different setup in Fig. 10b. In addition, the straightforward solution of only canceling the phase difference between the two computational states does not work for more than two qubits. When the number of qubits is higher, the seperation between the transitions becomes too small and unwanted transitions (rather than just phase differences) become the main sources of the gate error. A possible solution to this would be to have a better look at which qubit gate has the largest

gate error. Then by again comparing the effective Hamiltonians, an optimal pulse might be found which reduces the gate error of this 'problem' qubit gate. In order to overcome these limitations, in the next chapter we try to produce pulses with lower gate errors, by introducing new pulse shapes and using numerical optimization of pulse parameters.

4 Multiparameter semi-analytic pulses

4.1 Numerically optimized pulses

In the previous section we have looked at analytical existing pulse shapes with few parameters. These pulses are preferred by experimentalists because of the easy optimization procedure. Numerical optimized pulses however, have shown to give very low gate errors for single qubit gates [8], much lower than the DRAG pulse. The problem is that these numerical optimized pulses are not smooth (they are step functions, with very small time intervals on the order of 1 ns) and therefore hard to implement on the available waveform generators. The question is if there is an intermediate approach. We try to address this problem by using a semi-analytic pulse with enough parameters to cancel low order unwanted effects of off-resonant pulses, which can be implemented in experimental setups. In this chapter, we introduce this pulse and look at the gate errors which can be achieved using the analytical techniques from the previous chapter in combination with numerical optimization of the parameters. The idea is to use this pulse with many parameters on top of our improved pulse from the previous chapter. In this way, small corrections could be applied to a simple pulse, to lower the gate error.

4.2 The Irwin-Hall pulse

The basis for the many-parameter pulse will be the Irwin-Hall probability distribution, which is the distribution for the sum of n independent uniformly distributed random variables. The resulting probability function is a spline, that is a piecewise polynomial function, with n distinct pieces. [13]

The reason for using the Irwin-Hall distribution as basis for the pulse is that it starts and ends at zero (has no infinite tails), and has about the same shape as Gaussian (for $n \to \infty$, the Irwin-Hall distribution becomes a Gaussian), see Fig.14. Since Gaussian shapes fall off quickly in both the time and frequency domain, this implies that the Irwin-Hall distribution also falls off quickly in the frequency domain. This is needed since in practice, the pulses to drive qubits will be created using waveform generators with a finite frequency range. In particular the distribution for $n = 4$ is used, because it is one of the simplest ones for which the derivative is still smooth. This is useful in the optimization process.

The formula for Irwin-Hall (n=4):

$$I_4(t) = \begin{cases} 1/6t^3 & 0 \leq t \leq 1 \\ 1/6(-3t^3 + 12t^2 - 12t + 4) & 1 \leq t \leq 2 \\ 1/6(3t^3 - 24t^2 + 60t - 44) & 2 \leq t \leq 3 \\ 1/6(-t^3 + 12t^2 - 48t + 64) & 3 \leq t \leq 4 \end{cases}$$

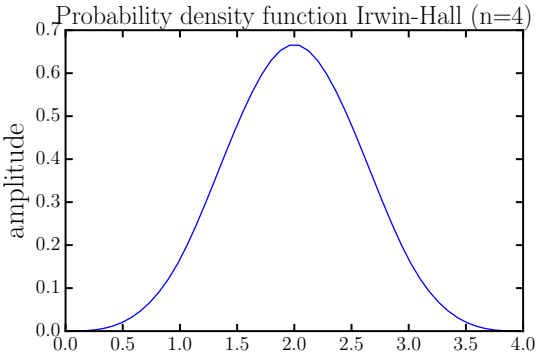

Figure 14: Graph of the probability density function of the Irwin-Hall distribution for $n = 4$

Starting from this expression, we construct Ω_x in the following way: Four I_4 pulses will be used subsequently, with different amplitudes a_0, a_1, a_2 and a_3. For a gate time of 10 (ns) this leads to the following graph for the pulse on the in-phase quadrature:

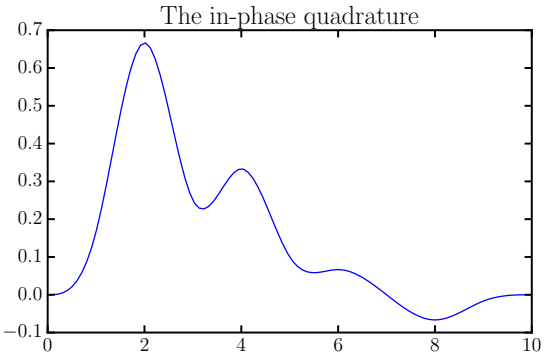

Figure 15: Graph of the pulse on the in-phase quadrature. Each I_4 pulse can have a different amplitude, possibly negative.

The pulse on the out-of-phase quadrature obeys exactly the same general formula, with possibly different amplitudes a_4, a_5, a_6 and a_7. This leads to the formula of this pulse, for an arbitrary gate time T:

$$\begin{aligned}\Omega_x &= a_0 I_4\left(\frac{10t}{T}\right) + a_1 I_4\left(\frac{10(t-2)}{T}\right) + a_2 I_4\left(\frac{10(t-4)}{T}\right) + a_3 I_4\left(\frac{10(t-6)}{T}\right)\\ \Omega_y &= a_4 I_4\left(\frac{10t}{T}\right) + a_5 I_4\left(\frac{10(t-2)}{T}\right) + a_6 I_4\left(\frac{10(t-4)}{T}\right) + a_7 I_4\left(\frac{10(t-6)}{T}\right)\end{aligned} \tag{4.1}$$

Note that with these formula's, there are four, partly overlapping, subsequent Irwin-Hall pulses on both the in- and out-of-phase quadrature. This is to 'divide' the 8 pulse parameters equally over the complete gate time. The reason for choosing 8 pulse parameters is that this number is higher than the number of free parameters which are needed to tune the Hamiltonian to make the final gate correct.
Again, we stress that the pulse which we described, will have low amplitudes and will be added to our improved pulse from the previous chapter.

4.3 Combining Irwin-Hall and analytic solutions

In the previous chapter we introduced improved analytic pulses (phase ramping) which produced qubit gates with significant lower errors than simple Gaussian pulses. We combine these pulses with the Irwin-Hall pulse by adding them up. This is illustrated in Fig. 16, for one of the two quadratures. Starting with all parameters of the Irwin-Hall pulse being 0, the numerical optimization process is used to find the small adjustments which are needed to lower the total gate error.

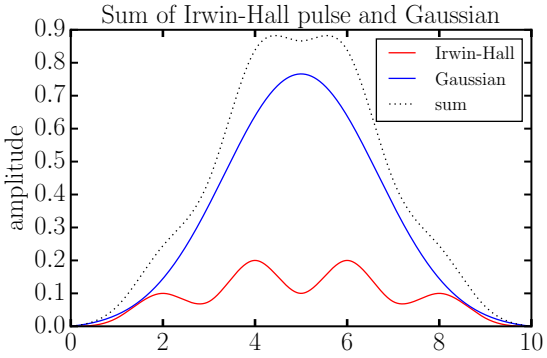

Figure 16: The black dotted graph is the sum of the Gaussian (blue solid) and Irwin-Hall (red solid) pulse.

We have seen that the additional Irwin-Hall pulse is completely described by the gate time T and 8 parameters. The final gate is completely described by the time propagator at the gate time T, $U_{\text{final}} = U(0, t_g)$
As described in Chapter 2, this thesis focuses on implementing the X-gate. For the numerical optimization it is important to specify the exact requirements this final gate. In the three dimensional Hilbert space, including the leakage level, this ideal gate is given by Eq. 2.12. It is important to note that this equation shows that we assume that the qubit as a whole may acquire an overall phase factor ϕ_1. In addition, the leakage level can acquire an arbitrary phase factor relative to the computational subspace of the system.

The exact optimization process for the multi-parameter Irwin-Hall pulse is described in Appendix E. The main idea is that the final time propagator depends on the input pulse parameters in an 'easy way', since the driving pulse is linear in the pulse parameters. Therefore the changes in the final gate as a result of changing the parameters (the partial derivatives of the final gate, with respect to the parameters) can be calculated. This makes that quick optimization using the root-finding Newton's method can be used for some situations. In situations in which this method does not converge, numerical (Python) optimization solvers are used to find the optimal set of parameters.

4.4 Results for single qubit gates

For a single qubit, Newton's method turns out to be a quick way of finding improved pulses, which result in lower gate errors for most gate times. An additional advantage is that this method leads to optimal solutions with small amplitudes for the added Irwin-Hall pulses. In Fig. 17 the gate errors of the simple Gaussian, the improve phase ramp pulse and the numerically optimized are plotted for different gate times. The amplitudes of the Irwin-Hall pulse which is added, are small. As an example, the optimal pulse for a gate time of 10 ns is shown in Fig. 18.

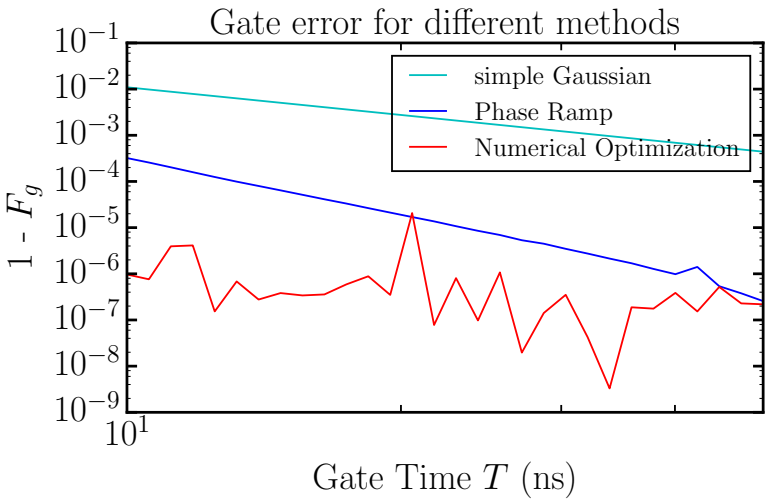

Figure 17: The gate errors for a simple Gaussian pulse, the phase ramp pulse and the numerically optimized pulse vs gate time

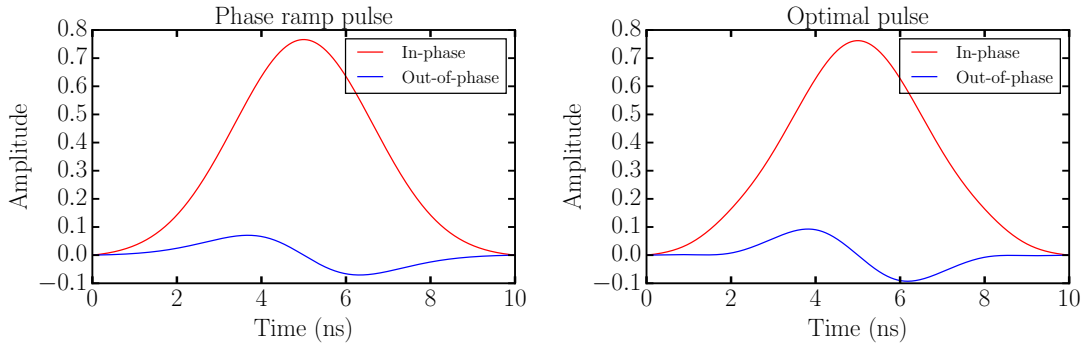

(a) *(b)*

Figure 18: The pulse in figure (a) is the optimal phase ramping pulse for a single qubit, as described in the previous chapter. After adding the small Irwin-Hall pulse and using numerical optimization, the new optimal pulse is given in figure (b). The coefficients for the optimal parameters $a_0, .., a_7$ are: [5.0, -1.9, -1.9, 5.3, -4.2, 6.0, -6.0, 4.2] ($\cdot 10^{-3}$) and we immediately see that the adjustments are small.

We see that the error is decreased by orders of magnitude for all gate times compared with the phase ramp pulse from the previous chapter. The large advantage of this combination pulse, is that it is still an analytical pulse. The large number of free parameters that can be used in the optimization process allows to reduce the error by a large amount.

4.5 Results for two-qubit gates

For the situation with two qubits, the frequency spectrum given in Fig. 10b, we can try the same approach. At both qubit frequencies ω_A and ω_B, we apply the combination of driving pulse from Sec 4.3. The optimization process is slightly adjusted, such that the optimal solution reduces the error for both qubit A and B at the same time. As it turns out, Newtons method does not work for this setup with two qubits. All results were obtained using the Python optimization process. As we can see in Fig. 19, the optimal pulses lead to enormous improvement compared to the analytical pulses from Chapter 3.

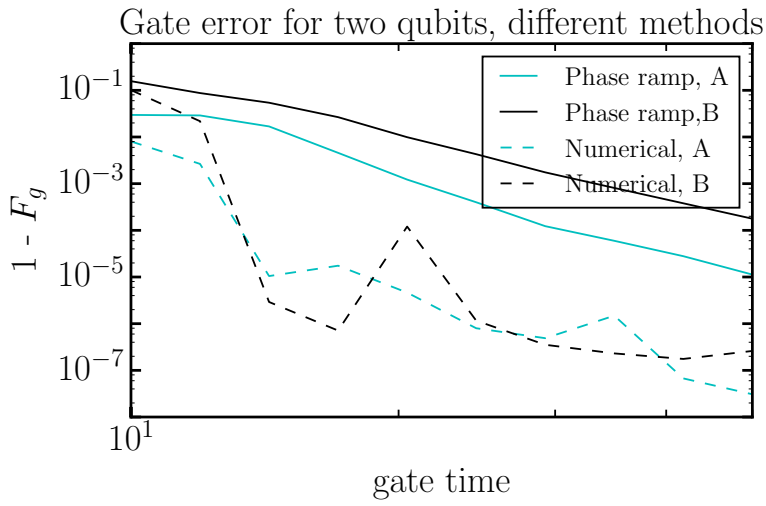

Figure 19: The solid lines give the gate errors for the gates on qubit A and B, when phase ramp pulses are used. The dashed lines give the gate errors for the numerically optimized pulses for both qubit A and B. For most gate times, the numerically optimized pulse gives very low gate errors.

4.6 Discussion of the results

For the single qubit gate, the optimization procedure leads to an optimal combination pulse with gate errors orders of magnitude lower than the current DRAG method and the phase ramp pulse. For a gate time of 10 ns, a gate error of 10^{-6} is obtained, compared to a gate error of 10^{-3} for the analytic phase-ramp pulse of this duration. The large advantage of this pulse compared with the numerical GRAPE pulses is that the basis of the pulse are simple analytic pulse shapes. The parameters of the pulse are just the amplitudes of these basic pulse shapes. The disadvantage of this pulse compared with for example the Wah-Wah pulse is the larger number of parameters. However, it could be worth trying to see if the experimental optimization procedure can be applied to this larger number of parameters.

For the two-qubit gate the results of the numerically optimized pulse look very promising as well. A two-qubit gate with an error of 10^{-4} or lower for both qubits could (theoretically) be obtained within 15 ns. This is a shorter gate time than the 17 ns for the

Wah-Wah pulse, which only performed an X-gate on one of the two qubits. The improvement is due to the larger set of parameters, which are harder to be implemented in experimental research. Another difference with the experiments reported in Ref. [11] is the larger seperation between the qubit transition frequencies. The smallest difference between two transitions is $\delta = 0.15$ GHz 2π, compared with $\delta = 0.045$ GHz 2π for the situation for which the Wah-Wah pulse is used. This is due to a new setup in which the frequency spectra of the different qubits are merged, which makes it possible to put more qubits within a given frequency bandwidth, avoiding very small seperations.

An open question is whether this approach can be extended to more than two qubits. Future research could focus on extending this semi-analytical approach to even more qubits. In addition, we have made some assumptions which are hard to defend and not realizable in practice. An example is that we tacitly assumed that all qubits couple equally to the driving pulse (a resonator in experiments). This is often not the case in experiments and could easily be taken into account in the simulations.

5 Conclusion and Outlook

In this thesis we have looked at performing multi-qubit gates in transmon systems. In order to understand the effects of and differences between off-resonant and on-resonant driving of a qubit, an adiabatic expansion was made. This expansion led to the important conclusion that for single qubits, gate errors are dictated by induced phase differences in the computational subspace. The standard Gaussian pulse shape is slightly adjusted, which cancels the phase differences between the different qubit levels. This solution is equivalent to an improved pulse from [9]. The result is that the gate errors for this improved pulse are comparable with the well known DRAG pulse [8].

In addition the expansion was used in combination with a new distribution of the qubit transitions in frequency space which avoids small separations between two qubits. Similar to the single qubit situation, the expansion was used to cancel unwanted phase differences between the energy levels for both qubits. Using two improved electromagnetic pulses simultaneously on the two qubits, gate errors decreased by 2 orders of magnitude for most gate times between 10 and 50 ns compared to simple pulses. Extending the analytical approach to more than two qubits is hard, since leakage, instead of phase shifts between levels, becomes the main source of the error. A crucial point is that the expansion breaks down for certain separations between the qubit transitions. It would be good to have a solution or alternative expansion which works for this separation of transition frequencies as well. In addition, future research could look better into the three-qubit situation and see which qubit (gate) has the largest gate error. All the other pulses could be shaped to decrease this larger error and thereby decrease the overall error, instead of using three pulses simultaneously which are optimal for single-qubit gates.

To reduce gate errors even more, a new pulse (Irwin-Hall pulse) with 8 parameters was introduced. The optimal amplitudes (parameters) were obtained by numerical optimization. This new pulse led to even lower gate errors for single-qubit gates than the DRAG pulses. In addition the approach gave low gate errors for applying two qubit gates at the same time. The gate errors for both qubits are as low as 10^{-4} for a gate time of just 15 ns. This sounds very promising and it should be tested to see whether these multi-parameter pulses are feasible in experimental research. Numerical optimization could be tested on a real qubit in the lab in the following way: all pulses could be calibrated using a program which uses as input all the qubit parameters, which are measured in advance, and then returns the optimal pulse parameters. We want to stress that the derivation of analytical pulse shapes gets harder as more qubits have to be taken into account and gate times get shorter. For gate times of several nanoseconds, the rotating wave approximation cannot always be made, which makes it even harder to find analytic optimal pulses. The effect of this approximation on the performance of analytically derived optimal pulses shapes for short gate times might be studied into more detail in the future.

A model of a physical system is never perfect. It is crucial to recognize and understand the differences between the model and the real transmon qubits in experiments. For real qubits, we have to deal with coupling to more leakage levels and a cavity which acts as a frequency filter. Another important difference between our model and the reality is the difference in coupling to the feedline for different qubits. This means that the transitions for one qubit are driven with lower-amplitude pulses than the transitions for the other qubit. An important next step in creating optimal pulses is to include these effects in the model. This will help us understand the experimental results better in the ongoing effort to find the optimal procedure to reduce gate errors.

Appendix A Basis transformation

We derive formula 2.5 for the Hamiltonian in an arbitrary rotating frame (obtained by a unitary transformation) given the Hamiltonian in a certain frame S.
Assume that transformation from a state $|\psi\rangle_s$ in frame S to the state $|\phi\rangle$ in the rotating frame is given by:

$$|\phi\rangle = U|\psi\rangle_S \tag{A.1}$$

which means that:

$$|\psi\rangle_S = U^\dagger|\phi\rangle \tag{A.2}$$

with U unitary.
The Schrödinger equation in frame S:

$$i\hbar\frac{\partial|\psi\rangle_S}{dt} = H_S|\psi\rangle_S \tag{A.3}$$

Likewise, the Schrödinger equation in the rotating frame is given by:

$$i\hbar\frac{\partial|\phi\rangle}{dt} = \tilde{H}|\phi\rangle \tag{A.4}$$

When we substitute equation (A.2) in equation (A.4) we get:

$$\begin{aligned}
i\hbar\frac{\partial}{dt}\left(U^\dagger|\phi\rangle\right) &= H_S U^\dagger|\phi\rangle \Leftrightarrow \\
i\hbar\left(\dot{U}^\dagger|\phi\rangle + U^\dagger\frac{\partial|\phi\rangle}{dt}\right) &= H_S U^\dagger|\phi\rangle \Leftrightarrow \\
i\hbar U^\dagger\frac{\partial|\phi\rangle}{dt} &= \left(-i\hbar\dot{U}^\dagger + H_S U^\dagger\right)|\phi\rangle \Leftrightarrow \\
i\hbar\frac{\partial|\phi\rangle}{dt} &= \left(UH_S U^\dagger - i\hbar U\dot{U}^\dagger\right)|\phi\rangle
\end{aligned}$$

Comparing this expression with equation (A.4), shows us that: $\tilde{H} = UH_S U^\dagger - i\hbar U\dot{U}^\dagger$.
Now using the fact that $\tilde{H}$ should be hermitian (and so is H_S) we get:

$$\tilde{H} = \tilde{H}^\dagger = UH_S U^\dagger + i\hbar\dot{U}U^\dagger \tag{A.5}$$

Appendix B Rotating Wave Approximation

In this section we explain concisely what the Rotating Wave Approximation (RWA) is and why we are allowed to make this approximation in deriving equation 2.6. We start with the equation of the Hamiltonian of the qubit under influence of an electromagnetic pulse in the labframe

$$\hat{H} = \hat{H}_0(t) + \hbar\Omega(t)\left(\sigma_1^+ + \sigma_1^- + \lambda(\sigma_2^+ + \sigma_2^-)\right). \tag{B.1}$$

When we apply the time-dependent unitary transformation 2.4 and use the equation for the Hamiltonian in the new frame 2.5, which is derived in appendix A, the full Hamiltonian in the rotating frame becomes:

$$\hat{H}^{RF} = \frac{\hbar}{2}\left[\left(\Omega_C^\dagger(t)e^{-i\delta_1 t} + \Omega_C(t)e^{-i(\omega_d+w_1)t}\right)\sigma_1^+ + \lambda\left(\Omega_C^\dagger(t)e^{-i\delta_2 t} + \Omega_c(t)e^{-i(\omega_1+\Delta+\omega_d)t}\right)\sigma_2^+\right] + h.c., \tag{B.2}$$

where $\delta_j = \omega_1 - \omega_d$, ω_d is the driving frequency, ω_1 is the qubit frequency and Δ the anharmonicity of the system.
For transmon qubits in experiments, the qubit frequency (and therefore the driving frequency) are on the order of several GHz [10]. The driving frequency ω_d is nearly on resonance with the qubit frequency ω_1. The result is that:

$$|\delta_1| << |\omega_1 + \omega_d|$$
$$|\delta_2| << |\omega_1 + \Delta + \omega_d|,$$

which means that some of the terms in the Hamiltonian oscillate much faster than others. The approximation we make, is that on the timescales at which the experiments take place (10 ns or longer, [10], these oscillating (rotating) terms quickly average to zero. The oscillating terms have a negligible influence on the final state of the system. This means that these terms can be neglected, which results in the simpler Hamiltonian in equation 2.6.

To validate this approximation, we calculate the squared norm of the difference time propagator U_d, which is given by

$$U_d = U_{\text{final, RWA}} - U_{\text{final, full}} \tag{B.3}$$

A plot of the squared norm of this difference time propagator gives an idea of the error which is introduced by using the Rotating Wave Approximation. In Fig. 20 squared norm of U_d is given for different gate times. It gives an indication with which order the errors introduced by the RWA scale.

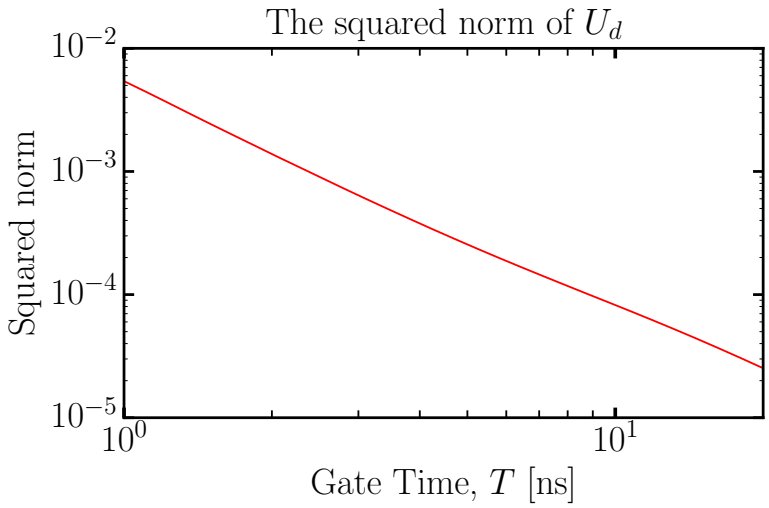

Figure 20: The squared norm of the difference time propagator U_d is plotted against the gate time T. A simple Gaussian pulse was used, with detuning $\delta = 0.1$ GHz $\cdot 2\pi$. The values give an indication of which errors are introduced by applying the RWA.

It is important to realize that for very short gate times, the RWA cannot always be applied. In this thesis we focus on multi-qubit gates with longer gatetimes (more than 10 ns), it should therefore be safe to apply the approximation.

Appendix C Commuting Hamiltonians

In this appendix we show that in the simple situation described in section 2.2, the time ordering operator in equation (2.9) can be dropped.
Resonance is assumed between driving frequency and qubit frequency, which means that $w_d = w_1$. In addition $\lambda = 0$ is set.
Substituting these simplifications in equation (2.7) gives the following Hamiltonian in the rotating frame:

$$\hat{H}^{RF}(t) = \frac{\hbar}{2}\begin{pmatrix} 0 & \Omega_C^\dagger(t) & 0 \\ \Omega_C(t) & 0 & 0 \\ 0 & 0 & 0 \end{pmatrix} \tag{C.1}$$

For the commutator of two Hamiltonians at times t_1 and t_2 this gives:

$$\begin{aligned}[H^{RF}(t_1), H^{RF}(t_2)] &= H^{RF}(t_1)H^{RF}(t_2) - H^{RF}(t_2)H^{RF}(t_1) \\ &= \begin{pmatrix} \Omega_C^\dagger(t_1)\Omega_C(t_2) - \Omega_C(t_1)\Omega_C^\dagger(t_2) & 0 & 0 \\ 0 & \Omega_C(t_1)\Omega_C^\dagger(t_2) - \Omega_C(t_1)^\dagger\Omega_C(t_2) & 0 \\ 0 & 0 & 0 \end{pmatrix}\end{aligned} \tag{C.2}$$

This expression is in general not equal to O (the zero matrix), when $\Omega_C = \Omega^x + i\Omega^y$ is complex. If we set $\Omega^y = 0$ and $\Omega^x = \Omega_\pi$ (Ω_π satisfying requirement (2.14)), the expression in equation (C.2) does become 0 for all times t_1, t_2.
For this specific case:

$$[H^{RF}(t_1), H^{RF}(t_2)] = 0 \tag{C.3}$$

Appendix D Effective Hamiltonian

We start with the differential equation:

$$\frac{dU}{dt} = -\frac{i}{\hbar}HU \tag{D.1}$$

With U being the time-propagator and H the Hamiltonian of the system. The solution to this equation is given by the Dyson series

$$U(t,t_0) = U_0(t,t_0) + U_1(t,t_0) + U_2(t,t_0) + U_3(t,t_0) + ..., \tag{D.2}$$

where

$$\begin{aligned} U_0 &= I \\ U_1(t,t_0) &= \int_{t_0}^{t} -\frac{i}{\hbar}H(t')\ \mathrm{d}t' \\ U_2(t,t_0) &= \int_{t_0}^{t} -\frac{i}{\hbar}H(t')U_1(t')\ \mathrm{d}t' \end{aligned} \tag{D.3}$$

We are going to approximate the timepropagator U to order $\frac{1}{T^2}$, with T the pulse duration. We do this by calculating $U(t,t_0)$ for a cleverly chosen t_p, the *averaging period*. We apply a on-resonant pulse to our qubit system, which we write as $\Omega_1(t) = \Omega_1^x(t) + i\Omega_1^y(t)$ The hamiltonian in the rotating frame (with respect to the qubit transitions) becomes:

$$H(t) = \frac{\hbar}{2}\begin{pmatrix} 0 & \Omega_1^*(t) & 0 \\ \Omega_1(t) & 0 & \lambda_1\Omega_1^*(t)e^{-i\Delta t} \\ 0 & \lambda_1\Omega_1(t)e^{i\Delta t} & 0 \end{pmatrix} \tag{D.4}$$

As an example of how the integrals are approximated, we show the calculation for $U_1(t)$.

D.1 Calculating $U_1(t)$

$\frac{dU_1}{dt} = -\frac{i}{\hbar}H$. For $t_0 < t < t_0 + t_p$ this gives:

$$U_1(t,t_0) = -\frac{i}{2}\begin{pmatrix} 0 & \int_{t_0}^{t}\Omega_1^*(t')\ \mathrm{d}t' & 0 \\ \int_{t_0}^{t}\Omega_1(t')\ \mathrm{d}t' & 0 & \int_{t_0}^{t}\lambda_1\Omega_1^*(t')e^{-i\Delta t'}\ \mathrm{d}t' \\ 0 & \int_{t_0}^{t}\lambda_1\Omega_1(t')e^{i\Delta t'}\ \mathrm{d}t' & 0 \end{pmatrix}. \tag{D.5}$$

In the integrals we approximate $\Omega(t) \approx \Omega(t_0) + \dot{\Omega}(t_0)(t - t_0)$. The next term in the Taylor expansion would contain a factor $\ddot{\Omega}(t_0)$. Since $\Omega \sim \frac{1}{T}$, we see that $\ddot{\Omega}(t) \sim \frac{1}{T^3}$. We do not take terms of this order into account in the expansion. Therefore, this expansion in $\Omega(t)$ should be enough.
When we use this approximation for Ω_1 we get:

$$
\begin{aligned}
\int_{t_0}^{t} \Omega_1^*(t')\ \mathrm{d}t' &= \Omega_1^*(t_0)(t-t_0) + \frac{1}{2}\dot{\Omega}_1^*(t_0)(t-t_0)^2 \\
\int_{t_0}^{t} \Omega_1(t')\ \mathrm{d}t' &= \Omega_1(t_0)(t-t_0) + \frac{1}{2}\dot{\Omega}_1(t_0)(t-t_0)^2 \\
\int_{t_0}^{t} \lambda_1\Omega_1^*(t')e^{-i\Delta t'}\ \mathrm{d}t' &= \lambda_1\Omega_1^*(t_0)\frac{1}{-i\Delta}(e^{-i\Delta t} - e^{-i\Delta t_0}) \\
&\quad + \lambda_1 e^{-i\Delta t_0}\dot{\Omega}_1^*(t_0)\left(\frac{e^{-i\Delta t}}{(-i\Delta)^2}(-i\Delta(t-t_0)-1) + \frac{1}{(-i\Delta)^2}1\right) \\
\int_{t_0}^{t} \lambda_1\Omega_1(t')e^{i\Delta t'}\ \mathrm{d}t' &= \lambda_1\Omega_1(t_0)\frac{1}{i\Delta}(e^{i\Delta t} - e^{i\Delta t_0}) + \lambda_1 e^{i\Delta t_0}\dot{\Omega}_1(t_0)\left(\frac{e^{i\Delta t}}{(i\Delta)^2}(i\Delta(t-t_0)-1) + \frac{1}{(i\Delta)^2}1\right)
\end{aligned}
\tag{D.6}
$$

Now comes the important step. We choose an averaging period, such that all oscillating terms in the above integrals average out. In this case $t_p = \frac{2\pi}{\Delta}$ suffices. For $U_1(t_0+t_p, t_0)$ we therefore approximate to $\mathcal{O}(\Omega^2) = \mathcal{O}(\frac{1}{T^2})$:

$$
U_1(t_0+t_p,t_0) = -\frac{i}{2}\begin{pmatrix} 0 & \Omega_1^*(t_0)t_p + \frac{1}{2}\dot{\Omega}_1^*(t_0)t_p^2 & 0 \\ \Omega_1(t_0)t_p + \frac{1}{2}\dot{\Omega}_1(t_0)t_p^2 & 0 & \lambda_1 e^{-i\Delta t_0}\dot{\Omega}_1^*(t_0)\frac{t_p}{-i\Delta} \\ 0 & \lambda_1 e^{i\Delta t_0}\dot{\Omega}_1(t_0)\frac{t_p}{i\Delta} & 0 \end{pmatrix}
\tag{D.7}
$$

In the same way, by approximating $\Omega(t)$ under each integral, $U_2(t_0+t_p,t_0)$ can be calculated as well. We do not need to calculate U_i for $i > 2$, since these would only contain terms of $\mathcal{O}(\Omega^3) = \mathcal{O}(\frac{1}{T^3})$.
At this point we have the expressions for $U_1(t_0+t_p,t_0)$, $U_2(t_0+t_p,t_0)$ up to second order in Ω. Since

$$
U(t_0+t_p,t_0) \equiv e^{-\frac{i}{\hbar}H_{\text{eff}}\cdot t_p},
\tag{D.8}
$$

we have using the Taylor Expansion of the logarithm

$$
\begin{aligned}
H_{\text{eff,on}} &= \frac{i\hbar\log(U)}{t_p} \\
&= \frac{i\hbar}{t_p}\log(I-(I-U)) \\
&\approx \frac{i\hbar}{t_p}\left(-(I-U) - \frac{1}{2}(I-U)^2\right) \\
&= \frac{i\hbar}{t_p}\left((U_1+U_2) - \frac{1}{2}(U_1+U_2)^2\right).
\end{aligned}
\tag{D.9}
$$

This gives the final expression for the effective Hamiltonian $H_{\text{eff,on}}$. The calculations for the off-resonant pulse are similar. The only difference is that there are more oscillating terms, which makes the choice for the averaging period t_p less trivial. For both the on-resonant and off-resonant pulse, the effective Hamiltonian will have to be validated numerically.

Appendix E The optimization process

E.1 The time propagator

In the section 4.1 a new multi-parameter pulse was introduced. The final gate is completely described by the time propagator at the gate time T, $U_T = U(0,T)$. In this chapter the outline of the numerical optimization procedure is given.
It begins with the Schrödinger equation:

$$\frac{d|\psi(t)\rangle}{dt} = \frac{-i}{\hbar}\hat{H}(t)|\psi(t)\rangle \tag{E.1}$$

where i is the imaginary unit, $\hbar$ is the Planck's constant h divided by 2π, H is the Hamiltonian of the system and $|\psi(t)\rangle$ is the state of the system at time t.

Since $|\psi(t)\rangle = U(0,t)|\psi(0)\rangle$ for all initial states $|\psi(0)\rangle$, this leads to a similar differential equation for the time propagator $U(0,t)$:

$$\frac{dU(0,t)}{dt} = \frac{-i}{\hbar}\hat{H}(t)U(0,t) \tag{E.2}$$

The final state of the system can be calculated by solving the (differential) Schrödinger equation (E.1) for a given initial state $|\psi_0\rangle$. The important step is that (when again using the eigenstates (energy states) of the qubit $|j\rangle$ as basis),

$$|\psi_0\rangle = |0\rangle = \begin{pmatrix}1\\0\\0\end{pmatrix}$$

leads to a final state $|\psi(T)\rangle$ which forms the first column of $U(0,T)$, the time-propagator for the system in matrix form. The complete time propagator can be found by calculating the final states at $t = T$ for
$|\psi_0\rangle = \begin{pmatrix}0\\1\\0\end{pmatrix}$ and $|\psi_0\rangle = \begin{pmatrix}0\\0\\1\end{pmatrix}$ as well.

Since the ideal gate in equation 2.12 can contain an arbitrary phase factor, a small trick is used to compare the final gate with the ideal gate. After calculating U_T, the phase factor ($\phi_{U_{10}}$) is 'removed' from the [1,0] element of the matrix (U_{10}). The part of the matrix which belongs to the computational subspace $U_{\mathrm{T,\ comp}}$, is multiplied with the same factor.

$$U_{\mathrm{final,comp}} = U_{\mathrm{T,\ comp}} e^{-i\phi_{U_{10}}} \tag{E.3}$$

The other entries of U_{final} ('outside' the computational subspace) are the same as the entries of U_T. The difference matrix D_U is then defined to be the difference between the calculated gate U_{final} and U_{ideal}.

$$D_U = U_{\mathrm{ideal}} - U_{\mathrm{final}} \tag{E.4}$$

The goal of the optimization process is to find the set of parameters which correspond to a pulse which produces U_{final} with a low error. This is equivalent to minimizing the sum of the (absolute value) of the entries of the matrix D_U. The lower the sum of the absolute value of these entries, the closer D_U is to the zero matrix. $D_U = 0$ means that $U_{\mathrm{ideal}} = U_{\mathrm{final}}$

E.2 The Jacobian

In order to improve the numerical optimization process, the Jacobian of U_{final} (U_f) with respect to the pulse parameters is added. There exists an analytical expression for the Jacobian of U_T using equation (E.5) and (E.2).

$$\begin{aligned}\frac{d}{dt}\left(\frac{\partial U_T}{\partial \alpha}\right) &= \frac{\partial}{\partial \alpha}\left(\frac{dU_T}{dt}\right) \\ &= \frac{\partial}{\partial \alpha}\left(\frac{-i}{\hbar}H(t)U_T(t)\right) \\ &= \frac{-i}{\hbar}\left(\frac{\partial H}{\partial \alpha}U_T(t) + H(t)\frac{\partial U_T}{\partial \alpha}\right)\end{aligned} \tag{E.5}$$

This expression in combination with the chain rule can be used to find the partial derivatives of U_{final} with respect to the pulse parameters as well.
α can be any of the 8 pulse parameters. This system of equations can be solved 'column by column'. Using a matrix equation which has the following structure. We illustrate this structure with an example with only the first two parameters to find the first column. $U_{a_0,10}$ denotes the [1,0] element of the matrix $\frac{\partial U_T}{\partial a_1}$.

$$\begin{pmatrix} U'_{00} \\ U'_{10} \\ U'_{20} \\ U'_{a_0,00} \\ U'_{a_0,10} \\ U'_{a_0,20} \\ U'_{a_1,00} \\ U'_{a_1,10} \\ U'_{a_1,20} \end{pmatrix} = \frac{-i}{\hbar} \left(\begin{array}{c|c|c} H & O & O \\ \hline \frac{\partial H}{\partial a_0} & H & O \\ \hline \frac{\partial H}{\partial a_1} & O & H \end{array}\right) \begin{pmatrix} U_{00} \\ U_{10} \\ U_{20} \\ U_{a_0,00} \\ U_{a_0,10} \\ U_{a_0,20} \\ U_{a_1,00} \\ U_{a_1,10} \\ U_{a_1,20} \end{pmatrix} \tag{E.6}$$

$\frac{\partial H}{\partial \alpha}$ are easy to calculate, since the multi-parameter pulse is linear in the parameters α. This gives

$$\frac{\partial H}{\partial \alpha} = \frac{\hbar}{2}\begin{pmatrix} 0 & P^\dagger_\alpha(t)e^{-i(\omega_1-\omega_d)t} & 0 \\ P_\alpha(t)e^{i(\omega_1-\omega_d)t} & 0 & \lambda P^\dagger_\alpha(t)e^{-i(\omega_1+\Delta-\omega_d)t} \\ 0 & P_\alpha(t)e^{i(\omega_1+\Delta-\omega_d)t} & 0 \end{pmatrix} \tag{E.7}$$

Where $P_\alpha = \frac{\partial \Omega_C}{\partial \alpha}$

When the system of differential equations (E.6) is solved, this gives $\frac{\partial U_T}{\partial \alpha}$. Using the chain rule $\frac{\partial U_f}{\partial \alpha}$ can be calculated

$$\begin{aligned}\frac{\partial U_f}{\partial \alpha} &= \frac{\partial}{\partial \alpha}\left(e^{-i\phi_{U_{10}}}U_T\right) \\ &= e^{-i\phi_{U_{10}}}\frac{\partial U_T}{\partial \alpha} + \frac{\partial e^{-i\phi_{U_{10}}}}{\partial \alpha}U_T \\ &= e^{-i\phi_{U_{10}}}\frac{\partial U_T}{\partial \alpha} - ie^{-i\phi_{U_{10}}}\frac{\partial \phi_{U_{10}}}{\partial \alpha}U_T \\ &= e^{-i\phi_{U_{10}}}\frac{\partial U_T}{\partial \alpha} - ie^{-i\phi_{U_{10}}}\frac{\partial \phi_{U_{10}}}{\partial U_{10}}\frac{\partial U_{10}}{\partial \alpha}U_T\end{aligned}$$

It is important to note the difference between $\frac{\partial U_T}{\partial \alpha}$, which is a matrix, and $\frac{\partial U_{10}}{\partial \alpha}$ which is a (complex) scalar. U_{10} is the [1,0] element of U_T.

$\frac{\partial U_f}{\partial \alpha}$ and $\frac{\partial U_{10}}{\partial \alpha}$ are known expressions when the system of equations is solved. $\frac{\partial \phi_{U_{10}}}{\partial U_{10}}$ is an expression which can be calculated using z = x + yi = (x,y):

$$\begin{aligned}\frac{\partial \phi}{\partial z} &= \frac{\partial \phi}{\partial (x,y)} \\ &= (\frac{-y}{y^2+x^2}, \frac{1}{x+\frac{y^2}{x}})\end{aligned}$$

E.3 Numerical optimization

As mentioned before, a simple Gaussian pulse will lead to a perfect $\sigma^x_{0,1}$ gate in the adiabatic limit. With this in mind, we expect that small adjustments to this simple pulse should be sufficient to lower the gate error. We use Newton's method to find the 'root' of the difference matrix. If all the entries of the difference matrix are zero, this means that $U_{\text{final}} = U_{\text{ideal}}$, which is the goal. To use Newton's method, we turn the complex difference matrix with 6 complex elements into a vector with 12 real entries. Every complex matrix element is split into its real and imaginary part.

Newton's method is used to find the roots of a (system of) function(s) ($\mathrm{F}(\mathbf{x}) = 0$). It is an iterative algorithm which uses the following formula:

$$x_{n+1} = x_n - J^{-1} x_n \tag{E.8}$$

When the starting conditions are 'good', the sequence of x_n's converges to the true root of the function. The function must have non-zero derivative in the root and the initial guess must be as close to the root as possible. In our case, we do not use the inverse of the Jacobian (12 * 8 matrix), but the Moore-Penrose Pseudo-inverse. We expect that the sequence of $x'_n s$ converges to the optimal set of parameters.

In addition the Scipy (Python) function optimize.root is used to find the root of the vector function (D_U matrix). This approach is used when Newton's method does not converge and therefore does not give a solution.

References

[1] H. Häffner, C. F. Roos, and R. Blatt. Quantum computing with trapped ions. *Physics Reports*, 469:155–203, December 2008.

[2] K. C. Nowack, F. H. L. Koppens, Y. V. Nazarov, and L. M. K. Vandersypen. Coherent Control of a Single Electron Spin with Electric Fields. *Science*, 318:1430–, November 2007.

[3] J. Koch, T. M. Yu, J. Gambetta, A. A. Houck, D. I. Schuster, J. Majer, A. Blais, M. H. Devoret, S. M. Girvin, and R. J. Schoelkopf. Introducing the Transmon: a new superconducting qubit from optimizing the Cooper Pair Box. *eprint arXiv:cond-mat/0703002*, February 2007.

[4] R. Shankar. *Principles of Quantum Mechanics*. Kluwer Academic/Plenum Publisher, New York, Second Edition edition, 1994.

[5] J. J. Sakurai. *Modern Quantum Mechanics (Revised Edition)*. Addison Wesley, 1 edition, September 1993.

[6] M. D. Bowdrey, D. K. L. Oi, A. J. Short, K. Banaszek, and J. A. Jones. Fidelity of single qubit maps. *Physics Letters A*, 294:258–260, March 2002.

[7] Bauer, C., Freeman, R., Frenkiel T., Keeler, J. and Shaka, A. J. Gaussian pulses. *Journal of Magnetic Resonance (1969)*, 58(3):442 – 457, 1984.

[8] F. Motzoi, J. M. Gambetta, P. Rebentrost, and F. K. Wilhelm. Simple Pulses for Elimination of Leakage in Weakly Nonlinear Qubits. *Physical Review Letters*, 103(11):110501, September 2009.

[9] J. M. Gambetta, F. Motzoi, S. T. Merkel, and F. K. Wilhelm. Analytic control methods for high-fidelity unitary operations in a weakly nonlinear oscillator. *Phys. Rev. A*, 83(1):012308, January 2011.

[10] J. M. Chow, L. DiCarlo, J. M. Gambetta, F. Motzoi, L. Frunzio, S. M. Girvin, and R. J. Schoelkopf. Optimized driving of superconducting artificial atoms for improved single-qubit gates. *Phys. Rev. A*, 82:040305, Oct 2010.

[11] R. Schutjens, F. A. Dagga, D. J. Egger, and F. K. Wilhelm. Single-qubit gates in frequency-crowded transmon systems. *Phys. Rev A*, 88(5):052330, November 2013.

[12] V. Vesterinen, O.-P. Saira, A. Bruno, and L. DiCarlo. Mitigating information leakage in a crowded spectrum of weakly anharmonic qubits. *ArXiv e-prints*, May 2014.

[13] Irwin-hall distribution — Wikipedia, the free encyclopedia, 2010. [Online; accessed 25-June-2015].